Article:

Liu, E-L, Yu, H-S, Zhou, C et al. (2 more authors) (2017) A Binary-Medium Constitutive Model for Artificially Structured Soils Based on the Disturbed State Concept and Homogenization Theory. International Journal of Geomechanics, 17 (7). 04016154. 04016154-04016154. ISSN 1532-3641

https://doi.org/10.1061/(ASCE)GM.1943-5622.0000859

A Binary-Medium Constitutive Model for Artificially Structured Soils Based on the Disturbed State Concept (DSC) and Homogenization Theory

En-Long Liu[1], Hai-Sui Yu[2], Cheng Zhou[1], Qing Nie[1], Kai-Tai Luo[1]

[1]State Key Laboratory of Hydraulics and Natural River Engineering, College of Water Resource and Hydropower, Sichuan University, Chengdu, P.R. China 610065

[2]Nottingham Centre for Geomechanics, University of Nottingham, NG7 2RD, UK; State Key Laboratory of Hydraulics and Natural River Engineering, Sichuan University, Chengdu, P.R. China 610065

Corresponding author: Cheng Zhou. Tel: +86 28 85405121. Email: geomanl@163.com.

Abstract: Triaxial compression tests were carried out on artificially structured soil samples at confining pressures of 25 kPa, 37.5 kPa, 50 kPa, 100 kPa, 200 kPa and 400 kPa. A binary-medium constitutive model for artificially structured soils is proposed based on the experimental results, the disturbance state concept (DSC) and homogenization theory. A new constitutive model for artificially structured soils was formulated by regarding the structured soils as a binary-medium consisting of bonded blocks and weakened bands. The bonded blocks are idealized as bonded elements whose deformation properties are described by elastic materials and the weakened bands are idealized as frictional elements whose deformation properties are described by the Lade-Duncan model. By introducing the structural parameters of breakage ratio and local strain coefficient, the non-uniform distribution of stress and strain within a representative volume element can be given based on the homogenization theory of heterogeneous materials. The methods for determination of the model parameters are given on the basis of experimental results. By making comparisons of predictions with experimental data, it is demonstrated that the new model provides satisfactory qualitative and quantitative modeling of many important features of artificially structured soils.

Key Words: artificially structured soils; binary-medium constitutive model; breakage ratio; local strain coefficient.

Introduction

Soils in situ usually possess natural structures, referring to the combination of fabric (arrangement of particles) and inter-particle bonding (Mitchell 1976), whose important influence on the mechanical features of soils has been recognized for a long time, enabling soils composed of the same materials to behave differently in a reconstituted state (Burland 1990; Leroueil and Vaughan 1990). The natural structure conveys extra strength to natural soils, allowing them to exist at a given stress. Upon loading, the bonds between soil particles may break, resulting in the so-called destructuration process. Until the present, research on the geotechnical engineering properties of reconstituted soils has been relatively satisfactory, and the modified Cam clay model (Schofield and Wroth 1968; Yao et al. 2009, 2015) and the Lade-Duncan model (Lade and Duncan 1975; Lade 1977) have been widely used in solving geotechnical problems resulting from reconstituted soils. It is widely known that the modified Cam clay model can simulate only the strain hardening and volumetric contraction of remolded clays relatively well but cannot well duplicate the strain softening and volumetric dilatancy of natural or structured soils at a low stress state under triaxial stress conditions (Smith et al. 1992). During the process of formation, natural soils are easily deposited layer by layer, which results in different mechanical properties in vertical and horizontal directions (Graham and Houlsby 1983). Therefore, when formulating the constitutive model of these types of soils, the influences of stress history, bonding, the fabric distribution and current stress state variables should be considered concurrently to describe the stress–strain properties well.

There have been important developments in formulating constitutive models incorporating the influence of soil structure based on comprehensive experimental studies on structured or natural soil. Many researchers have investigated the mechanical properties of structured soils by laboratory experiments on intact soil samples extracted from construction fields (Lo and Morin 1972; Sangrey 1972; Baracos et al. 1980; Schmertmann 1991; Diaz-Rodriguez et al. 1992; Callisto and Calabresi 1998; Cotecchia and Chandler 2000; Dudoignon et al. 2001; Callisto et al. 2002; Rocchi et al. 2013) and on artificially structured soils (Maccarini 1987; Bressani 1990; Malanraki and Toll 2001), in which the yielding, strength, deformation properties, aging, anisotropy, and stress path of structured soils were investigated. When formulating constitutive models for structured soils considering their mechanical properties obtained by laboratory experiments, there are some widely used methods, which include revising or reformulating the Cam clay model (Kavvads and Amorosi 2000; Asaoka et al. 2001; Liu and Carter 2002; Wheeler et al. 2003; Belokas and Kavvadas 2010; Suebsuk et al. 2011; Zhu and Yao 2013; Liu et al. 2011, 2013), damage mechanical model (Shen 1997; Zhao et al. 2002; Shen 2006;), DSC model (Liu et al. 2000; Liu et al. 2003) kinematic or bounding model (Rouainia and Wood 2000; Gajo and Wood 2001; Baudet and Stallebrass 2004; Huang et al. 2011) and micromechanical model (Yin et al. 2009; Gao and Zhao 2012). Many of these existing models are formulated based on macroscopic observation on stress-strain properties of structured soils and few can consider the physical and deformational mechanism of them. Furthermore, there is still no widely accepted constitutive model for structured soils at the moment.

Compared with the remolded clay, the structured soils behave with strain softening and volumetric contraction followed by dilatancy upon loading under a relatively low stress state, accompanying the appearance of the shear bands under triaxial and biaxial stress states. After the peak value of stress–strain curves of structured soils (Cotecchia and Chandler 2000), the yielding surface will contract gradually as a result of the breaking of bonds between soil particles, which makes it difficult to describe these phenomena using the conventional and widely employed elasto-plastic theory. Accompanying the bond breaking between soil particles, the stress and strain distributed within a soil element will not be uniform, and the higher local stress that equals the strength of the bonds will result in the breakup of these bonds between soil particles. Therefore, it is necessary to formulate a constitutive model for structured soils to consider the non-uniform stress and strain in the soil element and reflect the macroscopic strain softening by use of the parameters considering the micro deformation mechanism. Here, a new constitutive model for structured soils will be proposed to consider the damage process (or gradual bond breaking) and non-uniform distribution of strain (or stress) based on test results of artificially structured soils.

In this paper, the triaxial tests of artificially structured soils were performed at six different confining pressures ranging from 25 kPa to 400 kPa with drained conditions, and a theoretical study of the behavior of artificially structured soil is presented. Based on the homogenization theory of heterogeneous materials and the disturbance state concept (DSC), a new model, referred to as the binary-medium model for geological materials, is formulated by regarding the structured soils as a binary-medium consisting of bonded blocks and weakened bands. The determination of model parameters is provided and model verification is also made by comparison with the test results of artificially structured samples.

Test Conditions and Results

Sample Preparation

The artificially structured soils tested here are composed of silty clay, cement, kaolin clay and salt particles, in which silty clay is the main matrix material, cement can provide bonding between soil particles, kaolin clay can increase the content of fine particles of the samples, and salt particles can generate large pores within the samples by dissolving. The silty clay was extracted from one excavation pit located in Chengdu area, approximately 5 m below the ground surface, with blocky shape and slight moisture, and its G_s is 2.72. The grading curve of silty clay is shown in Fig. 1, and w_L and w_P are 29.11% and 17.06%, respectively. The silty clay is dried and sieved through a 0.5 mm screen and serves as the main matrix material mixed uniformly with other materials, including cement, kaolin clay and salt particles by mass (or weight), in which the mass ratios of silty clay, kaolin clay, cement and salty particle are 65%, 20%, 5% and 10%, respectively. The cement employed is 32.5R, which is produced in China. The uniform mixture is then compacted in a mold with the three same parts by five layers with dry density of 1.49 g/cm^3 to form the sample. The samples are vacuumed for approximately 3 h in a vacuum chamber before the distilled water flows in slowly. After the samples are soaked for 3 h, they are removed from the vacuum chamber and quickly placed in flowing water with a speed of 6.65 cm^3/s. After curing for seven days, the samples are taken from the mold and placed in the triaxial apparatus to be tested. During the process of curing, the salt content in the water is measured to ensure complete dissolution of the salt particles. Through seven days of curing, the salt content in the water surrounding the samples reaches its original value, which is equal to the magnitude of the flowing water; this demonstrates that salt particles are dissolved completely. The Scanning Electron Microscope (SEM) photo of one prepared sample is shown in Fig. 2, which presents the bonding between soil particles and the distribution of large pores within the sample. For natural soils, their main properties at the mesoscale are bonding and fabric (Burland 1990). In the process of preparing the samples, the hydration of cement generates some materials bonding soil particles together, and the dissolution of salt particles forms the large pores within the samples; thus, the initial isotropic structured samples will be prepared.

To investigate the influence of structure deterioration on the mechanical properties of soils, the remolded samples are also prepared here, and their preparing method is described as follows. The artificially structured samples tested are remolded, dried and sieved through a 0.5-mm screen. After that, the soils are compacted in the mold with five layers to form remolded samples with the same dry density as the structured ones. Obviously, the bonding between soil particles of the remolded samples is broken completely.

Test Results and Analysis

Triaxial compression tests under consolidated-drained conditions are conducted on both the artificially prepared samples and the remolded ones. The confining pressures applied are 25 kPa, 37.5 kPa, 50 kPa, 100 kPa, 200 kPa and 400 kPa, and loading rate is 0.06 mm/min. The apparatus employed is a GCTS triaxial system.

The deviatoric stress–axial strain curves and the volumetric strain–axial strain curves of the structured samples are presented in Fig. 3 (a)–(b), respectively, in which "S-CD-xx kPa" means that the structured sample is tested under consolidated-drained conditions at the confining pressure of xx kPa. From Fig 3 (a) and (b), we can find that (i) under lower confining pressures, the samples exhibit strain-softening behavior and initially contract followed by dilatancy, and the lower the confining pressure, the more the sample dilates; (ii) under higher confining pressures, the samples exhibit strain-hardening behavior and contract at all times, and the larger the confining pressure, the more the sample contracts. When the confining pressures are 25 kPa, 37.5 kPa, and 50 kPa, the bonds between soil particles at the end of consolidation are hardly damaged, so these bonds should be destroyed gradually during the application of shear loading, which causes the samples to exhibit strain softening behavior accompanied by the appearance of shear bands as shown in Fig. 4 (a)–(c). Conversely, when the confining pressures are 100 kPa, 200 kPa and 400 kPa, the bonds between soil particles at the end of consolidation are heavily damaged, so the sliding of the soil particles mainly contributes to their strength during the application of shear loading, which causes the samples to exhibit strain hardening behavior and contract accompanied by a failure pattern of bulging in the middle, as shown in Fig. 4 (d)–(f).

The deviatoric stress–axial strain–volumetric strain curves of the remolded samples are presented in Fig. 5 (a)–(b), in which R denotes the remolded samples. Because the bonds between soil particles of the remolded samples are very weak, their mechanical properties are distinct from those of artificially structured samples. From Fig. 5 (a) and (b), we can find that (i) the remolded samples exhibit strain hardening behavior under the confining pressures ranging from 25 kPa to 400 kPa; and (ii) at low confining pressures, they contract first and then finally tend to dilate with the overall volumetric compaction, and at high confining pressures, they contract at all times. When remolding the artificially structured samples in the process of preparation, the bonds between soil particles break to form larger aggregates that are composed of the remolded samples, which thus behave as coarse-grained soils (Yu 2006). The failure patterns of remolded samples are in the form of bulges in the middle, as shown Fig. 6 (a)–(f) under all confining pressures.

From the test results of the structured samples and remolded ones under consolidated-drained conditions with different confining pressures, we can find that (i) under the relatively lower confining pressures, the deviatoric stresses of the structured samples are larger than those of remolded samples, as shown in Fig. 7 for the confining pressure of 50 kPa. The artificially structured soils exhibit strain-softening behavior, but the remolded samples exhibit strain hardening behavior; (ii) under the relatively higher confining pressures, both types of samples exhibit strain hardening behavior. In the process of strain hardening, the deviatoric stresses of the structured samples are larger than those of the remolded samples, and the differences between them are decreasing, as shown in Fig. 8 for the confining pressure of 200 kPa; and (iii) under the confining pressures ranging from 25 kPa to 400 kPa, the volumetric compaction of the remolded samples is larger than that of the structured samples.

Binary-medium Constitutive Model for Artificially Structured Soils

Breakage Mechanism of Structured Soils

Soil structures have a great influence on the mechanical properties of natural soils (Mitchell 1976), in which the cohesive resistance and frictional resistance contribute together to the bearing capacity of the soil element. It has also been long known that cohesive and frictional resistance are not mobilized simultaneously at different deformation or strain levels (Lambe 1960), with the former reaching a peak value within a relatively small strain and the latter making a full contribution within a relative large deformation or strain. It is obvious that the cohesive component exhibits brittle behavior and the frictional component exhibits nonlinear elastic behavior. The cohesion essentially comes from the cementation bonding between particles, whose distribution is not uniform among geological materials. The bonded blocks are formed where the cementation bonding strength is stronger, and the weakened bands are formed where the cementation bonding is weaker, so the heterogeneous structured soils are developed step by step via sedimentation. During the loading process, the brittle bonded blocks gradually break up, transforming to elasto-plastic weakened bands, so the two components bear the loading collectively. With the development of the breakage process, the bearing capacity of the bonded blocks will decrease, and that of the weakened bands will increase; however, the structured soil wholly exhibits strain hardening or strain softening behavior, depending on the increase of the bearing capacity of the weakened bands and the decrease of the bearing capacity of the bonded blocks. In view of the understanding of the breakage mechanism of structured soils mentioned previously, the structured soil can be conceptualized as a binary-medium material consisting of bonded blocks and weakened bands bearing the capacity collectively (Shen 2006). In the following, the bonding blocks are called the bonded elements, and the weakened bands are called frictional elements. There are similar concept of Disturbed State Concept (DSC) proposed by Desai and coworkers (Liu et al. 2000; Desai 1974, 2001), in which the continuum element is assumed to be composed of intact (RI) and adjusted (FA) states and has been used for soils (sands and clays), rocks, rockfill, asphalt, concrete, silicon, polymers, and interfaces and joints. In DSC, a deforming material is a mixture of (RI and FA states and similar in bonded materials) components which interact with each other to lead to the observed behavior. The material mixture can undergo degradation or softening and stiffening or healing. However, the basis in the damage approach is different; it starts from the assumption that a part of the material is damaged or cracked. The observed behavior is then defined based essentially on behavior of the undamaged part, and both do not interact because the damaged part is assumed to possess no strength.

Fig. 9 presents the sketch of Binary-Medium, where the bonded element is composed of a spring (E_b) and a brittle bond (q) and the frictional element is composed of a spring (E_f) and a plastic slider (f). For the brittle bond, it does not deform when the stress is less than the bond strength q and fail once the stress reaches q. In a continuum of structured soil sample, there are many bonded elements and frictional elements. Upon loading, some bonded elements may break up and transfer to frictional elements and bear external loads collectively.

Formulation of Binary-medium Constitutive Model for Artificially Structured Soils

The stress–strain relation of artificially structured soils, regarded as a binary-medium material consisting of bonded elements and frictional elements, can be derived by taking a representative volume element (RVE) based on homogenization theory for heterogeneous materials (Wang et al. 2002) as follows.

For a representative volume element, or RVE, the local stress and local strain are denoted by σ_{ij}^{loc} and ε_{ij}^{loc}, respectively, and thus both the average stress σ_{ij} and the average strain ε_{ij} can be written as follows:

$$\sigma_{ij} = \frac{1}{V}\int \sigma_{ij}^{loc}\mathrm{d}V \tag{1}$$

$$\varepsilon_{ij} = \frac{1}{V}\int \varepsilon_{ij}^{loc}\mathrm{d}V \tag{2}$$

where V is the volume of the RVE and loc represents local stress or strain.

σ_{ij}^{b} and σ_{ij}^{f} are defined as the stresses of bonded elements and frictional elements, respectively, and they have the following expressions:

$$\sigma_{ij}^{b} = \frac{1}{V_b}\int \sigma_{ij}^{loc}\mathrm{d}V_b \tag{3}$$

$$\sigma_{ij}^{f} = \frac{1}{V_f}\int \sigma_{ij}^{loc}\mathrm{d}V_f \tag{4}$$

where V_b and V_f are the volumes of bonded elements and frictional elements in the RVE, respectively, and b and f represent the bonded and frictional elements, respectively. From equation (1), we have

$$\sigma_{ij} = \frac{1}{V}\int \sigma_{ij}^{loc}dV = \frac{V_b}{V}\sigma_{ij}^{b} + \frac{V_f}{V}\sigma_{ij}^{f} \tag{5}$$

ε_{ij}^{b} and ε_{ij}^{f} are defined as the strains of bonded elements and frictional elements, respectively, with the following expressions:

$$\varepsilon_{ij}^{b} = \frac{1}{V_b}\int \varepsilon_{ij}^{loc}\mathrm{d}V_b \tag{6}$$

$$\varepsilon_{ij}^{f} = \frac{1}{V_f}\int \varepsilon_{ij}^{loc}\mathrm{d}V_f \tag{7}$$

From equation (2), we have

$$\varepsilon_{ij} = \frac{1}{V}\int \varepsilon_{ij}^{loc}dV = \frac{V_b}{V}\varepsilon_{ij}^{b} + \frac{V_f}{V}\varepsilon_{ij}^{f} \tag{8}$$

Setting λ as a breakage ratio, the ratio of volume of frictional elements to the whole volume of RVE is expressed as follows:

$$\lambda = \frac{V_f}{V} \tag{9}$$

Substituting Eq. (9) into Eqs. (5) and (8), we can express the average stress and average strain as follows:

$$\sigma_{ij} = (1 - \lambda)\sigma_{ij}^{b} + \lambda\sigma_{ij}^{f} \tag{10}$$

$$\varepsilon_{ij} = (1 - \lambda)\varepsilon_{ij}^{b} + \lambda\varepsilon_{ij}^{f} \tag{11}$$

The breakage ratio is changing with strain level upon loading, which is an internal variable similar to the damage factor used in damage mechanics or hardening parameter used in plasticity. We assume here that the breakage ratio is a function of strain, namely,

$$\lambda = f(\varepsilon_{ij}) \tag{12}$$

By use of Eq. (10), we can obtain the incremental expression of the stress as follows:

$$d\sigma_{ij} = (1 - \lambda^{0})d\sigma_{ij}^{b} + \lambda^{0}d\sigma_{ij}^{f} + d\lambda(\sigma_{ij}^{f0} - \sigma_{ij}^{b0}) \tag{13}$$

where λ^{0} is the current breakage ratio, and σ_{ij}^{b0} and σ_{ij}^{f0} are the current stresses of bonded elements and frictional elements, respectively. Similarly, by derivation of Eq. (11), we can obtain the incremental expression of the strain as follows:

$$d\varepsilon_{ij} = (1 - \lambda^{0})d\varepsilon_{ij}^{b} + \lambda^{0}d\varepsilon_{ij}^{f} + d\lambda(\varepsilon_{ij}^{f0} - \varepsilon_{ij}^{b0}) \tag{14}$$

where ε_{ij}^{b0} and ε_{ij}^{f0} are the current strains of bonded elements and frictional elements, respectively.

The tangential stiffness matrixes of bonded elements and frictional elements are represented by D_{ijkl}^{b} and D_{ijkl}^{f}, respectively, so we have the following stress–strain relationships for bonded elements and frictional elements:

$$d\sigma_{ij}^{b} = D_{ijkl}^{b}d\varepsilon_{kl}^{b} \tag{15}$$

and

$$d\sigma_{ij}^{f} = D_{ijkl}^{f}d\varepsilon_{kl}^{f} \tag{16}$$

By manipulation of Eq. (14), we have

$$d\varepsilon_{ij}^{f} = \frac{1}{\lambda^{0}}\{d\varepsilon_{ij} - (1 - \lambda^{0})d\varepsilon_{ij}^{b} - d\lambda(\varepsilon_{ij}^{f0} - \varepsilon_{ij}^{b0})\} \tag{17}$$

Substituting Eq. (17) into Eq. (16), we can obtain

$$d\sigma_{ij}^{f} = \frac{1}{\lambda^0} D_{ijkl}^{f}\{d\varepsilon_{kl} - (1-\lambda^0)d\varepsilon_{kl}^{b} - d\lambda(\varepsilon_{kl}^{f0} - \varepsilon_{kl}^{b0})\} \tag{18}$$

Combing Eq. (13) and Eq. (18), we can have the following equation expressed as

$$\begin{aligned} d\sigma_{ij} = {} & (1-\lambda^0)\{D_{ijkl}^{b} - D_{ijkl}^{f}\}d\varepsilon_{kl}^{b} + D_{ijkl}^{f}d\varepsilon_{kl} - d\lambda D_{ijkl}^{f}\{\varepsilon_{kl}^{f0} - \varepsilon_{kl}^{b0}\} \\ & + d\lambda\{\sigma_{ij}^{f0} - \sigma_{ij}^{b0}\} \end{aligned} \tag{19}$$

We introduce the local strain coefficient C_{ijkl} to establish the relationship between the strain of bonded elements and the average strain of RVE as follows:

$$\varepsilon_{ij}^{b} = C_{ijkl}\varepsilon_{kl} \tag{20}$$

The incremental form of Eq. (20) is expressed as

$$d\varepsilon_{ij}^{b} = C_{ijkl}^{0}d\varepsilon_{kl} + dC_{ijkl}\varepsilon_{kl}^{0} \tag{21}$$

where C_{ijkl}^{0} is the current local strain coefficient matrix. Substituting Eq. (21) into Eq. (19) with some manipulation, we can obtain

$$\begin{aligned} d\sigma_{ij} = {} & \{(1-\lambda^0)\{D_{ijmn}^{b} - D_{ijmn}^{f}\}C_{mnkl}^{0} + D_{ijkl}^{f}\}d\varepsilon_{kl} - d\lambda D_{ijkl}^{f}\{\varepsilon_{kl}^{f0} - \varepsilon_{kl}^{b0}\} \\ & + d\lambda\{\sigma_{ij}^{f0} - \sigma_{ij}^{b0}\} + (1-\lambda^0)\{D_{ijmn}^{b} - D_{ijmn}^{f}\}dC_{mnkl}\varepsilon_{kl}^{0} \end{aligned} \tag{22}$$

For the current stress and strain states, from Eqs. (10) and (11), we can obtain

$$\sigma_{ij}^{f0} = \frac{\sigma_{ij}^{0} - \left(1-\lambda^0\right)\sigma_{ij}^{b0}}{\lambda^0} \tag{23}$$

and

$$\varepsilon_{ij}^{f0} = \frac{\varepsilon_{ij}^{0} - \left(1-\lambda^0\right)\varepsilon_{ij}^{b0}}{\lambda^0} \tag{24}$$

where σ_{ij}^{0} and ε_{ij}^{0} are the current stress and strain of RVE, respectively.

Substitution Eqs. (23) and (24) into Eq. (22) with some manipulations, we can obtain the general stress–strain relationship as follows:

$$\begin{aligned} d\sigma_{ij} = {} & \{(1-\lambda^0)\{D_{ijmn}^{b} - D_{ijmn}^{f}\}C_{mnkl}^{0} + D_{ijkl}^{f}\}d\varepsilon_{kl} + (1-\lambda^0)\{D_{ijmn}^{b} - D_{ijmn}^{f}\}dC_{mnkl}\varepsilon_{kl}^{0} \\ & - \frac{d\lambda}{\lambda^0}D_{ijkl}^{f}\{\varepsilon_{kl}^{f0} - \varepsilon_{kl}^{b0}\} + \frac{d\lambda}{\lambda^0}\{\sigma_{ij}^{0} - \sigma_{ij}^{b0}\} \end{aligned} \tag{25}$$

At the initial loading, we have $\lambda^0 = 0$, $\{\varepsilon\}^0 = 0$, $\{\varepsilon\}_{\mathrm{b}}^0 = 0$ and $\{\varepsilon\}_{\mathrm{f}}^0 = 0$, which can be substituted into Eq. (22) to obtain the following stress expression at initial loading:

$$d\sigma_{ij} = \{(1-\lambda^0)\{D^b_{ijmn} - D^f_{ijmn}\}C^0_{mnkl} + D^f_{ijkl}\}d\varepsilon_{kl} + (1-\lambda^0)\{D^b_{ijmn} - D^f_{ijmn}\}dC_{mnkl}\varepsilon^0_{kl} \qquad (26)$$

In Eq. (25), there are four sets of parameters that must be determined, which include the constitutive relationship of bonded elements and frictional elements, breakage parameter and local strain matrix, which will be described in the following sections.

Constitutive Relationship of Bonded Elements

The bonded elements have bonding and large pores within them, whose behavior is similar to that of artificially structured soils at the initial loading within very small strain with almost intact structures. Natural soils are formed in layers by sedimentation, whose mechanical properties are isotropic in horizontal planes and different in horizontal and vertical directions. Therefore, we assume here that the bonded elements are cross-anisotropic elastic materials. When setting the symmetry axis along the z direction and the x axis and y axis in the horizontal plane, the stress–strain relationship, Eq. (15), of the bonded elements can be rewritten in Cartesian coordinates as follows:

$$\begin{Bmatrix} d\sigma_x \\ d\sigma_y \\ d\sigma_z \\ d\tau_{yz} \\ d\tau_{zx} \\ d\tau_{xy} \end{Bmatrix}_b = \begin{bmatrix} D_{11} & D_{12} & D_{13} & 0 & 0 & 0 \\ D_{12} & D_{11} & D_{13} & 0 & 0 & 0 \\ D_{13} & D_{13} & D_{33} & 0 & 0 & 0 \\ 0 & 0 & 0 & D_{44} & 0 & 0 \\ 0 & 0 & 0 & 0 & D_{44} & 0 \\ 0 & 0 & 0 & 0 & 0 & \dfrac{(D_{11} - D_{12})}{2} \end{bmatrix}_b \begin{Bmatrix} d\varepsilon_x \\ d\varepsilon_y \\ d\varepsilon_z \\ d\varepsilon_{yz} \\ d\varepsilon_{zx} \\ d\varepsilon_{xy} \end{Bmatrix}_b \qquad (27)$$

where the five material constants D_{11}, D_{12}, D_{13}, D_{33} and D_{44} can be determined by the stress–strain curves at the initial loading stage of the tested samples, during which the structured samples are hardly damaged and could be regarded as bonded elements. When $D_{11}= D_{33}$, $D_{12}= D_{13}$ and $D_{44}=(D_{11}- D_{12})/2$, Eq. (27) can be reduced to the stress–strain relationship of isotropic materials with two constants (Graham and Houlsby 1983).

Constitutive Relationship of Frictional Elements

The frictional elements are transformed from bonded elements when the bonds between soil particles are broken completely, whose mechanical properties could be assumed as those of remolded soils. From the test results of the remolded soils shown in Fig. 7 (a)–(b), we know that the stress–strain relationship of frictional elements can be described by the Lade-Duncan model (Lade and Duncan 1975; Lade 1977). For the Lade-Duncan model, the incremental strain of soils consists of elastic and plastic components in matrix form as follows:

$$\{d\varepsilon\}_f = \{d\varepsilon^e\}_f + \{d\varepsilon^p\}_f \tag{28}$$

where $\{d\varepsilon^e\}_f$ is the incremental elastic strain and $\{d\varepsilon^p\}_f$ is the incremental plastic strain.

According to the Lade-Duncan model, the elastic strain can be expressed as follows:

$$\begin{Bmatrix} d\varepsilon_x^e \\ d\varepsilon_y^e \\ d\varepsilon_z^e \\ d\varepsilon_{yz}^e \\ d\varepsilon_{zx}^e \\ d\varepsilon_{xy}^e \end{Bmatrix}_f = \frac{1}{E_f} \begin{Bmatrix} d\sigma_x - \nu_f(d\sigma_y + d\sigma_z) \\ d\sigma_y - \nu_f(d\sigma_z + d\sigma_x) \\ d\sigma_z - \nu_f(d\sigma_x + d\sigma_y) \\ 2(1+\nu_f)d\tau_{yz} \\ 2(1+\nu_f)d\tau_{zx} \\ 2(1+\nu_f)d\tau_{xy} \end{Bmatrix}_f \tag{29}$$

where E_f and ν_f are the tangential deformational modulus and tangential Poisson ratio of the remolded samples, respectively. In the Lade-Duncan model, the failure criterion is $f_1 = I_1^3 / I_3 = K_f$, the yielding function is $f = I_1^3 / I_3 = K_0$, and the plastic potential $\mathrm{g} = \mathrm{I}_1^3 - \mathrm{K}_2\mathrm{I}_3$, where I_1 and I_3 are the first invariant and third invariant of stress, respectively, and $K_f=K_0$ at failure. Therefore, according to the hardening elasto-plastic theory, we can obtain the incremental plastic strain as follows:

$$\begin{Bmatrix} d\varepsilon_x^p \\ d\varepsilon_y^p \\ d\varepsilon_z^p \\ d\varepsilon_{yz}^p \\ d\varepsilon_{zx}^p \\ d\varepsilon_{xy}^p \end{Bmatrix}_f = d\vartheta \cdot K_2 \begin{Bmatrix} \dfrac{3I_1^2}{K_2} - \sigma_y\sigma_z + \tau_{yz}^2 \\ \dfrac{3I_1^2}{K_2} - \sigma_z\sigma_x + \tau_{zx}^2 \\ \dfrac{3I_1^2}{K_2} - \sigma_x\sigma_y + \tau_{xy}^2 \\ 2\sigma_x\tau_{yz} - 2\tau_{xy}\tau_{zx} \\ 2\sigma_y\tau_{zx} - 2\tau_{xy}\tau_{yz} \\ 2\sigma_z\tau_{xy} - 2\tau_{yz}\tau_{zx} \end{Bmatrix}_f \tag{30}$$

where $d\vartheta$ is the plastic multiplier and K_2 is the model constant. A detailed description of the Lade-Duncan model can be found in the literature (Lade and Duncan 1975; Lade 1977).

Structural Parameters of Breakage Ratio and Local Strain Coefficient Matrix

The breakage ratio λ is a structural parameter whose evolving rules are closely related to soil type, stress and strain level, stress path and history. At the initial stage of loading, λ is very small with a value close to zero for the external loads, which are mainly borne by the bonded elements. With the process of loading, λ increases gradually, accompanied by bonded elements transferring to frictional elements, both of which bear the external loading. When the strain is very large, λ tends to be 1.0, and the external loads are mainly borne by frictional elements at the moment. In view of the determination method of the damage factor and hardening parameters (Krajcinovic and Mastilovic 1995; Yu 2006), we assume that the breakage ratio λ is a function of volumetric strain and generalized shear strain with the following expression:

$$\lambda = 1 - \exp\left(-\beta(\alpha\varepsilon_z + \varepsilon_x + \varepsilon_y)^{\psi} - (\xi\varepsilon_s)^{\theta}\right) \tag{31}$$

where $\varepsilon_s = \sqrt{2e_{ij}e_{ij}/3}$, $e_{ij} = \varepsilon_{ij} - \varepsilon_{kk}\delta_{ij}/3$, δ_{ij} is the Kronecker delta，and α, β, ξ, ψ and θ are material parameters, with the symmetry axis along the z direction and the x axis and y axis in the horizontal plane.

The local strain coefficient bridges the strains of bonded elements and RVE, which can vary in the process of loading and be affected by loading history and strain level. We assume here that in the elements the local strain coefficient are the same and are represented by C of a function of generalized shear strain as follows:

$$C = \exp\left(-(t_c \times \varepsilon_s)^{r_c}\right) \tag{32}$$

where t_c and r_c are model parameters.

The breakage ratio and local strain coefficient are both internal variables, which should be determined by meso-mechanics at the mesoscale. However, it is very difficult to determine the meso parameters for structured soils, so here we establish their evolving relationships using similar determination methods of hardening parameters in plasticity or damage factors in damage mechanics. Based on the analysis of the breakage mechanism of artificially structured soils from mesoscale to macroscale, we formulate their expressions in which those model parameters could be determined by test results.

Determination of Model Parameters under Triaxial Stress Conditions

Under conventional triaxial stress conditions in which two types of soil samples including initially isotropic structured and the remolded samples previously mentioned are tested, the vertical direction is set as the z axial direction, along which the maximal principal stress is applied, and the other two principal stresses are applied in the horizontal plane. Combining the test results provided above, we present the determination method of the model parameters under triaxial stress conditions in the following sections.

(a) Parameter Determination for Bonded Elements

Under conventional triaxial stress conditions, the stress–strain relationship of bonded elements, Eq. (27), can be simplified as follows:

$$\begin{Bmatrix} d\sigma_1 \\ d\sigma_3 \end{Bmatrix}_b = \frac{E_{vb}}{(1-\nu_{hhb})E_{vb} - 2\nu_{vhb}^2 E_{hb}} \begin{bmatrix} (1-\nu_{hhb})E_{vb} & 2\nu_{vhb}E_{hb} \\ \nu_{vhb}E_{hb} & E_{hb} \end{bmatrix} \begin{Bmatrix} d\varepsilon_1 \\ d\varepsilon_3 \end{Bmatrix}_b \tag{33}$$

where there are four material parameters, E_{vb}, E_{hb}, ν_{vhb} and ν_{hhb}, where E_{vb} and E_{hb} represent the elastic moduli of bonded elements in the vertical and horizontal directions, respectively, and ν_{vhb} and ν_{hhb} represent the Poisson ratios of bonded elements in the vertical and horizontal directions, respectively.

Within a small strain range upon initial loading, there are mainly bonded elements in RVE to bear the external loads, so the stress–strain curve of the structured samples can be very similar to that of bonded elements. Here, we use the strain of 0.25% of the artificially structured samples tested to determine E_{vb}, E_{hb}, ν_{vhb} and ν_{hhb}. Using Eq. (33), we can solve for only the values of E_{vb} and ν_{vhb}. For initially stress-induced anisotropic structured samples, when $E_{vb} = E_{hb}$ and $\nu_{vhb} = \nu_{hhb}$, they become initially isotropic structured samples. E_{vb}, E_{hb}, ν_{vhb} and ν_{hhb} are functions of confining pressure σ_3 expressed as $E_{vb}(\text{or } E_{hb}) = b_1 \ln\left(\frac{\sigma_3}{p_a}\right) + b_2$ and $\nu_{hhb}(\text{or } \nu_{vhb}) = b_3\left(\frac{\sigma_3}{p_a}\right)^{b_4}$, where b_1, b_2, b_3, and b_4 are material constants, and p_a is the atmospheric pressure of 0.1014 MPa.

(b) Parameter Determination for Frictional Elements

Frictional elements are transferred from bonded elements and bonding between soil particles that are fully breaking up, whose mechanical properties are similar to those of remolded soils and can be described by the Lade-Duncan model (Lade and Duncan 1975; Lade 1977) as mentioned above. Based on the test results of the remolded soils, we give the parameters of the Lade-Duncan model here.

Under conventional triaxial stress conditions, Eq. (28) can be rewritten as follows:

$$\begin{Bmatrix} d\sigma_1 \\ d\sigma_3 \end{Bmatrix}_f = [D]_f^{ep} \begin{Bmatrix} d\varepsilon_1 \\ d\varepsilon_3 \end{Bmatrix}_f \tag{34}$$

where $[D]_f^{ep}$ is the stiffness matrix of the frictional elements. According to the Lade-Duncan model, the elastic parameters of E_f and ν_f can be determined by the nonlinear elastic model of the Duncan-Chang hyperbolic model (Lade and Duncan 1975; Lade 1977) as follows:

$$\mathrm{E_f} = \mathrm{Kp_a}\left(\frac{\sigma_3}{\mathrm{p_a}}\right)^{\mathrm{n}}\left[1-\frac{\mathrm{R_f}(\sigma_1-\sigma_3)(1-\sin\varphi)}{2\mathrm{c}\cos\varphi+2\sigma_3\sin\varphi}\right]^2 \tag{35}$$

and

$$\nu_{\mathrm{f}} = \frac{\mathrm{G}-\mathrm{F}\lg(\sigma_3/\mathrm{p_a})}{\left\{1-\dfrac{\mathrm{D}(\sigma_1-\sigma_3)}{\mathrm{Kp_a}\left(\dfrac{\sigma_3}{\mathrm{p_a}}\right)^{\mathrm{n}}\left[1-\dfrac{\mathrm{R_f}(\sigma_1-\sigma_{33})(1-\sin\varphi)}{2\mathrm{c}\cos\varphi+2\sigma_3\sin\varphi}\right]}\right\}^2} \tag{36}$$

where K, n, R_f, G, F and D are material constants, and c and φ are the cohesion and internal frictional angles of the remolded soils, respectively; the stress is that of the frictional elements.

By setting $\mathrm{m_1} = \dfrac{\mathrm{E_f}(1-\nu_{\mathrm{f}})}{(1+\nu_{\mathrm{f}})(1-2\nu_{\mathrm{f}})}$, we can present $[D]_f^{ep}$ as follows:

$$[D]_f^{ep} = \begin{bmatrix} m_1 - \dfrac{n_3}{n_9} & \dfrac{2m_1\nu_f}{1-\nu_f} - \dfrac{n_4}{n_9} \\ \dfrac{m_1\nu_f}{1-\nu_f} - \dfrac{n_5}{n_9} & \dfrac{m_1}{1-\nu_f} - \dfrac{n_6}{n_9} \end{bmatrix} \tag{37}$$

where

$$\mathrm{n_1} = \mathrm{m_1}(3\mathrm{I_1^3} - \mathrm{K_2}\sigma_3^2 + \frac{2\nu_{\mathrm{f}}}{1-\nu_{\mathrm{f}}}(3\mathrm{I_1^2} - \mathrm{K_2}\sigma_1\sigma_3)) \tag{38-1}$$

$$\mathrm{n_2} = \mathrm{m_1}(\frac{\nu_{\mathrm{f}}}{1-\nu_{\mathrm{f}}}(3\mathrm{I_1^3} - \mathrm{K_2}\sigma_3^2) + \frac{1}{1-\nu_{\mathrm{f}}}(3\mathrm{I_1^2} - \mathrm{K_2}\sigma_1\sigma_3)) \tag{38-2}$$

$$n_3=\frac{m_1^2\times n_1}{I_3^2}\left[(3I_1^3I_3-\sigma_3^2I_1^3)+\frac{\nu_f}{1-\nu_f}(3I_1^3I_3-\sigma_1\sigma_3I_1^3))\right] \tag{38-3}$$

$$n_4=\frac{m_1^2\times n_1}{I_3^2}\left[\frac{2\nu_f}{1-\nu_f}(3I_1^3I_3-\sigma_3^2I_1^3)+\frac{1}{1-\nu_f}(3I_1^3I_3-\sigma_1\sigma_3I_1^3))\right] \tag{38-4}$$

$$n_5=\frac{m_1^2\times n_2}{I_3^2}\left[(3I_1^3I_3-\sigma_3^2I_1^3)+\frac{\nu_f}{1-\nu_f}(3I_1^3I_3-\sigma_1\sigma_3I_1^3))\right] \tag{38-5}$$

$$n_6=\frac{m_1^2\times n_2}{I_3^2}\left[\frac{2\nu_f}{1-\nu_f}(3I_1^3I_3-\sigma_3^2I_1^3)+\frac{1}{1-\nu_f}(3I_1^3I_3-\sigma_1\sigma_3I_1^3))\right] \tag{38-6}$$

$$n_7=\frac{m_1}{I_3^2}\left[(3I_1^3I_3-\sigma_3^2I_1^3)+\frac{\nu_f}{1-\nu_f}(3I_1^3I_3-\sigma_1\sigma_3I_1^3))\right] \tag{38-7}$$

$$n_8=\frac{m_1}{I_3^2}\left[\frac{2\nu_f}{1-\nu_f}(3I_1^3I_3-\sigma_3^2I_1^3)+\frac{1}{1-\nu_f}(3I_1^3I_3-\sigma_1\sigma_3I_1^3))\right] \tag{38-8}$$

$$n_9=\frac{\left[1-\beta'\left(f-f_t\right)\right]\sigma_3}{\alpha'}\frac{m_1}{I_3^2}\left[n_7(3I_1^2-K_2\sigma_3^2)+n_8(3I_1^2-K_2\sigma_1\sigma_3))\right] \tag{38-9}$$

and the stresses in these expressions are those of the frictional elements. K_2 and stress level f have the relationship shown in Fig. 10, which can be expressed as follows:

$$K_2=Af+27(1-A) \tag{39}$$

where A is the materials constant and f has the relationship with the plastic work as shown in Fig. 11, which can be expressed as follows:

$$f-f_t=\frac{W_p}{\alpha'+\beta' W_p} \tag{40}$$

where f_t=27 for the remolded soils tested, and α', β' are model parameters. Under conventional triaxial stress conditions, we have $f=\frac{\left[\left(\sigma_1-\sigma_3\right)+3\sigma_3\right]^3}{\left[\left(\sigma_1-\sigma_3\right)+\sigma_3\right]\sigma_3^{\,2}}$ and $W_p=\int\sigma_{ij}d\varepsilon_{ij}^p$. Substituting f, f_t and W_p into Eq. (40), we can obtain β' =0.01 and α' varying with the confining pressure as $\alpha'=r_1\left(\frac{\sigma_3}{p_a}\right)+r_2$, where r_1 and r_2 are material constants.

(c) Parameter Determination for Structural Parameters

Under conventional triaxial stress conditions, the breakage ratio λ of Eq. (31) can be written as

$$\lambda = 1 - \exp\left\{ -\beta(\alpha\varepsilon_1 + 2\varepsilon_3)^{\psi} - \left(\xi \frac{2}{3} (\varepsilon_1 - \varepsilon_3) \right)^{\theta} \right\} \tag{41}$$

For the artificially structured soils, the parameters β and ψ are constants; α, ξ and θ vary with the confining pressure by $\alpha(\text{or} \quad \xi, \theta) = e_1 \left(\frac{\sigma_3}{p_a} \right)^{e_2}$, where e_1 and e_2 are constants.

The local strain coefficient of C in Eq. (32) can be expressed under triaxial stress conditions as follows:

$$C = \exp\left\{ - \left(t_c \frac{2}{3} (\varepsilon_1 - \varepsilon_3) \right) \right\} \tag{42}$$

where $t_c = s_1 \left(\frac{\sigma_3}{p_a} \right) + s_2$, and s_1 and s_2 are constants.

Model Verification

There are four sets of parameters, including those of bonded elements, frictional elements, and structural parameters of breakage ratio and local strain coefficient, that must be provided in the proposed binary-medium constitutive model for artificially structured soils. These model parameters are determined for the samples tested as explained in Section "Test Conditions and Results" as follows.

For the bonded elements, the parameters are obtained as follows: b_1=9.8383 and b_2=30.37 for E_{vb}, b_1=9.1511 and b_2=28.61 for E_{hb}, b_3=0.2134 and b_4=-0.41 for ν_{hhb}, and b_3=0.1389 and b_4=-0.668 for ν_{vhb}.

For the frictional elements, the parameters are obtained as follows: K=88.797, n=0.3425, R_f =0.95, G=0.242, F=0.313, D=0.0113, c=0, φ=32.062° and A=0.3535; r_1=-14.0, r_2=-10.0 when σ_3<100 kPa and r_1=-155.0, r_2=-66.67 when $\sigma_3 \geq$100 kPa.

For the structural parameters, ψ is 1.0 and β =0.4 at σ_3<100 kPa and β =0.5 at $\sigma_3 \geq$100 kPa; when determining α, e_1=100.55, e_2=0.1135; when determining ξ, e_1=40.56, e_2=40.0 at σ_3<100 kPa and e_1=2.535, e_2=100.0 at $\sigma_3 \geq$100 kPa; when determining θ, e_1=0.0, e_2=0.15 at σ_3<100 kPa and e_1=0.0435, e_2=0.325 at $\sigma_3 \geq$100 kPa; and s_1=11.859, s_2=30.854.

The curves of deviatoric stress–axial strain and volumetric strain–axial strain of artificially structured soils computed and tested are shown in Fig. 12 and Fig. 13. From the deviatoric stress–axial strain curves shown in Fig. 12 (a) and Fig. 13 (a), although there are some slight differences in the values computed and tested, the proposed constitutive model can reflect the deformational features of artificially structured soils. At low confining pressures of 25 kPa, 37.5 kPa and 50 kPa, the computed results exhibit strain-softening behavior, which is in agreement with tested soils and whose peak values are very close to those of the tested results; at 100 kPa of confining pressure, both the computed and tested deviatoric stresses reach the plastic flow state simultaneously; at high confining pressures of 200 kPa and 400 kPa, the computed results exhibit strain-hardening behavior, which is also in agreement with the tested soils. From the volumetric strain–axial strain curves shown in Fig. 12 (b) and Fig. 13 (b), the computed results have similar properties to those of the tested soils. At low confining pressures of 25 kPa, 37.5 kPa and 50 kPa, the computed volumetric strains first contract and then dilate, with slightly larger values of contraction than those of the tested soils and very close dilatancy at failure; at high confining pressures of 100 kPa, 200 kPa and 400 kPa, both results computed contract continuously until failure, which agrees with the tested results with slight differences in values.

Discussions

The performance of the model for zero breakage states and completely broken sates are discussed here. For zero breakage states, the bonded elements are assumed to be elastic state in the paper and bear the external loading. Therefore, the structured soil sample can be represented by the bonded elements for zero breakage states. When determining the parameters of the bonded elements, the artificially structured soils at the initial loading within very small strain (e.g. 0.25% axial strain) are used to assure that the bonds between soil particles are in elastic state and not broken. For completely broken states, the bonded elements are wholly broken and transformed into frictional elements. Therefore, the structured soil sample can be represented by the frictional elements for completely broken states which bear the external loading. When determining the parameters of the frictional elements, the remolded soil sample prepared by remolding the artificially structured sample tested with dried and sieved through a 0.5 mm screen are used to assure that the bonds between soil particles are completely broken. For the micromechanical model for structured soil proposed here, the structured soil sample at failure usually consists of two components or binary media of bonded elements and frictional elements, and at failure the frictional elements dominate.

The relation between the proposed model and the bonded materials under the DSC are discussed here. In the references of Desai (2001) and Liu et al. (2000), it is assumed that the RI represents “zero strain state,”i.e., it is characterized as a perfectly rigid material. In the paper, however, the bonded elements are assumed to be elastic materials and can be transformed to be frictional elements denoted by the evolution of breakage ratio. For structured or cemented materials, Desai and coworkers (Desai 2001; Liu et al. 2000) only presented the constitutive model in one-dimensional formulation. In the paper, however, we give the generalized stress-strain equation for artificially structured soils and can be verified in triaxial tested results of artificially structured soil samples. And thus, the model proposed here is based on the disturbed state concept (DSC) and homogenization theory.

Conclusions

Artificially structured soil samples are tested under consolidated-drained conditions at confining pressures of 25 kPa, 37.5 kPa, 50 kPa, 100 kPa, 200 kPa and 400 kPa. Based on these test results, a binary-medium constitutive model for artificially structured soils is proposed in the manuscript. The conclusions can be drawn as follows.

(i) At low confining pressures of 25 kPa, 37.5 kPa and 50 kPa, the artificially structured soil samples exhibit strain-softening behavior and first contracts followed by dilatancy accompanying shear bands at failure; at 100 kPa confining pressure, the deviatoric stress increases gradually and reaches a plastic flow state and contracts during shear with a bulge in the middle at failure; at high confining pressures of 200 kPa and 400 kPa, all samples exhibit strain-hardening behavior and contract with a bulge in the middle at failure.

(ii) The new constitutive model, the binary-medium constitutive model proposed here for artificially structured soils, idealizes the structured samples as compositions of bonded elements described by elastic materials and frictional elements described by the Lade-Duncan model, whose distribution of stress and strain can be considered by introducing a local strain coefficient and breakage ratio. The computed results compared with the tested ones demonstrate that the new model can grasp the main mechanical properties of artificially structures soils including strain-softening and contraction followed by dilatancy at low confining pressures and strain-hardening and continuous contraction at high confining pressures.

Acknowledgments

The authors thank the reviewers and Editor very much for their comments and appreciate the financial support from the National Natural Science Foundation of China (NSFC) (Grant No. 51009103 and 51579167).

References

Asaoka, A., Nakano, M., and Noda, T. (2001). "The decay of structure and the loss of overconsolidation." Proc., 15th Int. Conf. on Soil Mechanics and Geotechnical Engineering, Lisse, 19-22.

Baracos, A., Graham, J., and Domaschuk, L. (1980). "Yielding and rupture in a Lacustrine clay." Can. Geotech. J.,, 17, 559-553.

Baudet, B., and Stallebrass, S. (2004). "A constitutive model for structured clays." Géotechnique, 54, 269-278.

Belokas, G., and Kavvadas, M. (2010). "An anisotropic model for structured soils." Comput. Geotech., 37, 737-747.

Bressani, L. A. (1990). "Experimental properties of bonded soils." PhD thesis, University of London, London.

Burland, J.B. (1990). "On the compressibility and shear strength of natural clays." Géotechnique, 40, 329-378.

Callisto, L., and Calabresi, G. (1998). "Mechanical behaviour of a natural soft clay." Géotechnique, 48, 495-513.

Callisto, L., Gajo, A., and Wood, D.M.(2002). "Simulation of triaxial and true triaxial tests on natural and reconstituted Pisa clay." Géotechnique, 52, 649-666.

Cotecchia, F., and Chandler, R.J. (2000). "A general framework for the mechanical behaviour of clays." Géotechnique, 50, 431-447.

Desai, C.S. (1974), "A consistent finite element technique for work-softening behaviour". Proc. Int. Conference on Computational Methods in Nonlinear Mechanics, Oden J. T. et al (eds), University of Texas, Austin, 969-978.

Desai, C.S. (2001). Mechanics of Materials and Interfaces: The Disturbed State Concept, CRC Press, Boca Raton.

Diaz-Rodriguez, J. A., Leroueil, S., and Aleman, J. D.(1992). “Yielding of Mexico city and other natural clays.” J. Geotech. Eng., 118, 981-995.

Dudoignon, P., Pantet, A., Carra, L., and Velde, B. (2001). “Macro-micro measurement of particle arrangement in sheared kaolinitic matrices.” Géotechnique, 51, 493-499.

Gajo, A., and Wood, D.M. (2001). “A new approach to anisotropic, bounding surface plasticity: general formulation and simulations of natural and reconstituted clay behavior.” Int.J. Numer. Anal. Meth. Geomech., 25, 207-241.

Gao, Z., and Zhao, J. (2012). “Constitutive modelling of artificially cemented sand by considering fabric anisotropy.” Comput.Geotech., 41, 57-69.

Graham, J., and Houlsby, G.T. (1983). “Anisotropic elasticity of a natural clay.” Géotechnique, 33, 165-180.

Huang, M., Liu, Y., and Sheng, D. (2011). “Simulation of yielding and stress-strain behavior of shanghai soft clay.” Comput. and Geotech., 38, 341-353.

Kavvads, M., and Amorosi, A. (2000). “A constitutive model for structured soils.” Géotechnique, 50, 263-273.

Krajcinovic, D., and Mastilovic, S. (1995). “Some fundamental issues of damage mechanics.” Mechanics of Materials, 21, 217-230.

Lade, P.V., and Duncan, J.M. (1975). “Elasto-plastic stress-strain theory for cohesionless soil.” J. Geotech. Engin. Divi., 101,1037-1053.

Lade, P.V. (1977). “Elasto-plastic stress-strain theory for cohesionless soil with curved yield surfaces.” Int.J. Solids Structures,13,1019-1035.

Lambe, T.W. (1960). “A mechanical picture of shear strength in clay.” In Research Conference on Shear Strength of Cohesive Soils. University of Colorado, Colorado, 555-580.

Leroueil, S., and Vaughan, P.R. (1990). “The important and congruent effects of structure in natural soils and weak rocks.” Géotechnique, 40,467-488.

Liu, M.D., and Carter, J.P. (2002). “A structured cam-clay model.” Can. Geotech. J., 39,1313-1332.

Liu, M.D., Carter, J.P., and Airey, D.W. (2011). "Sydney Soil model: (I) theoretical formulation." International J. of Geomechanics, ASCE, 11(3), 211-224.

Liu, M.D., Carter, J.P., and Desai, C.S. (2003). “Modelling compression behavior of structured geomaterials.” Int. J. Geomech., 3,191-204.

Liu, M.D., Carter, J.P., Desai, C.S., and Xu, K.J. (2000). “Analysis of the compression of structured soils using the disturbed state concept.” Int.J. Numer. Anal. Meth. Geomech. 24, 723-735.

Liu, W., Shi, M., Miao, L., Xu, L., and Zhang, D. (2013). “Constitutive modelling of the destructuration and anisotropy of natural soft clay.” Comput. Geotech., 51, 24-41.

Lo, K.Y., and Morin, J.P. (1972). “Strength anisotropy and time effects of two sensitive clays.” Can. Geotech. J., 9, 261-277.

Maccarini, M. (1987). “Laboratory studies of a weakly bonded artificial soil.” PhD thesis, University of London, London.

Malanraki, V., and Toll, D. G. (2001). “Triaxial tests on weakly bonded soil with changes in stress path.” J. of Geotech. and Geoenv. Eng., 127, 282-291.

Mitchell, J. K. (1976). Fundamentals of soil behavior, Wiley, New York.

Rocchi, G., Vaciago, G., Fontana, M., and Prat, M.D. (2013). “Understanding sampling disturbance and behavior of structured clays through constitutive modelling.” Soils Found., 53, 315-334.

Rouainia, M., and Wood, D.M. (2000). “A kinematic hardening constitutive model for natural clays with loss of structure.” Géotechnique, 50,153-164.

Sangrey, D. (1972). “On the causes of natural cementation in sensitive soils.” Can. Geotech. J., 9, 117-119.

Schmertmann, J.H. (1991). “The mechanical aging of soils.” J. of Geotech. Eng., 117, 1288-1330.

Schofield, A.N., and Worth, C.P.(1968). Critical State Soil Mechanics. MacGraw-Hill, London.

Shen, Z. J. (1997). “Development of structural model for soils.” Proc.,9th Conf. on Computational Methods and Advance in Geomechics, China, 1997, 235-240.

Shen, Z. J. (2006). “Progress in binary medium modeling of geological materials.” In Modern Trends in Geomechancis (Wu, W. and Yu, H.S. (Eds)), Springer: Berlin, 77-99.

Smith, P.R., Jardine, R.J., and Hight, D.W.(1992). “On the yielding of Bothkennar clay.” Géotechnique, 42, 257-274.

Suebsuk, J., Horpibulsuk, S., and Liu, M.D. (2011). “A critical sate model for overconsolidated structured clays.” Comput.Geotech., 38, 648-658.

Wang, J.G., Leung, C.F., and Ichicawa, Y. (2002). “A simplified homogenization method for composite soils.” Comput.Geotech., 29, 477-500.

Wheeler, S.J., Näätänen, A., Karstunen, M., and Lojander, M. (2003). “An anisotropic elastoplastic model for soft clays.” Can. Geotech. J., 40, 403-418.

Yao, Y.P., Hou, W., and Zhou, A. N. (2009). “UH model: three-dimensional unified hardening model for overconsolidated clays.” Géotechnique, 59, 451-469.

Yao, Y.P., Kong, L.M., Zhou, A.N., and Yin, J.H. (2015). “Time-dependent unified hardening model: three-dimensional elasto-visco-plastic constitutive model for clays.” ASCE, Journal of Engineering Mechanics,141(6), 04014162.

Yin, Z.Y., Chang, C.S., Hicher, P.Y., and Karstunen, M. (2009). “Micromechanical analysis of kinematic hardening in natural clay.” Int. J. Plast., 25, 1413-1435.

Yu, H.S. (2006). Plasticity and Geotechnics, Springer Publisher, Berlin.

Zhao, X.H., Sun, H., and Lo, K.W.(2002). “An elastoplastic damage model of soil.” Géotechnique 52, 533-536.

Zhu, E.Y., and Yao, Y.P. (2013). “A Structured UH Model.” In Constitutive modelling of geomaterials (Yang, Q. et al. (Eds)) ,Springer-Verlag: Berlin, 675-689.

List of figures

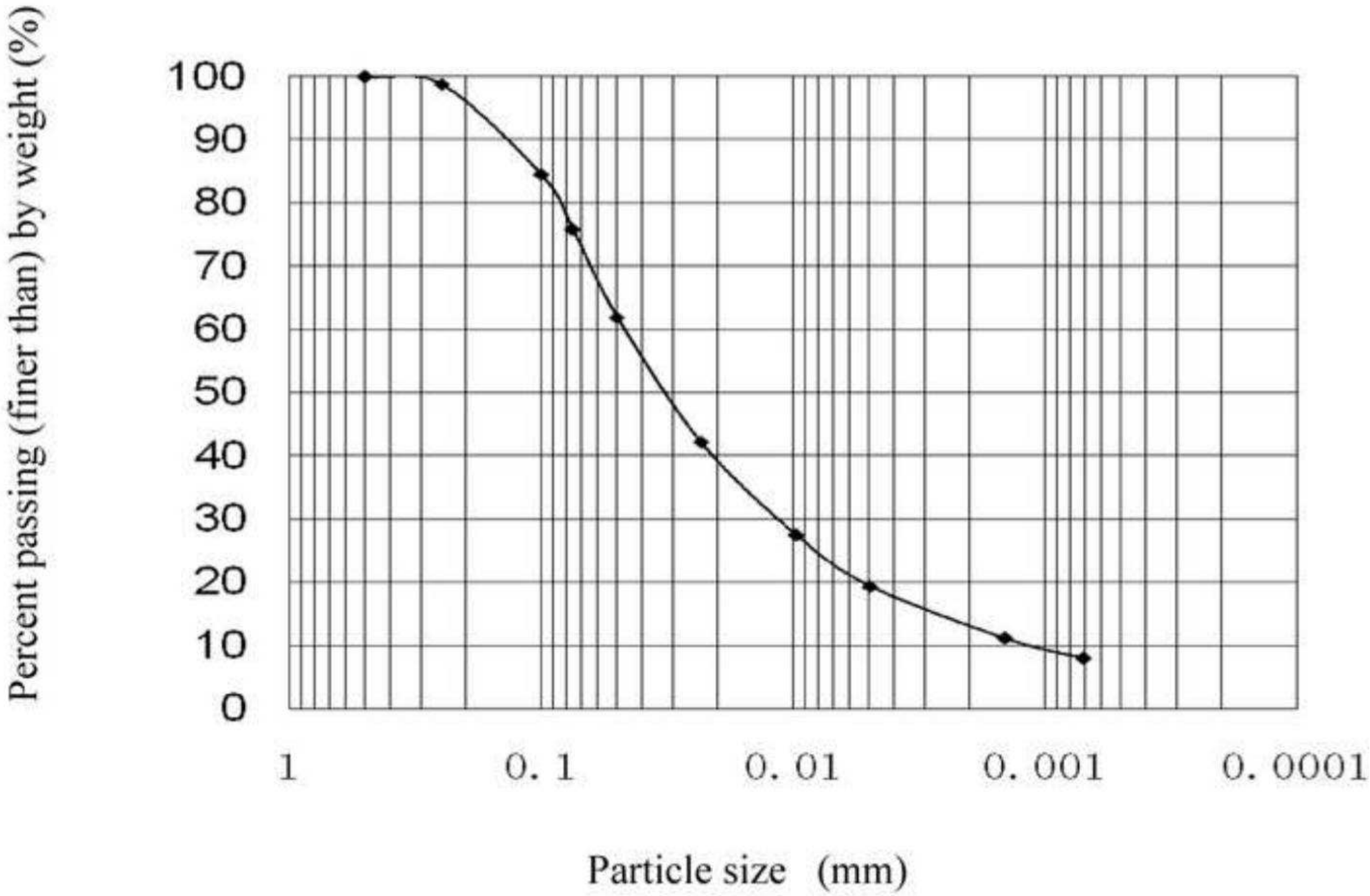

Fig. 1 Particle size distribution curve

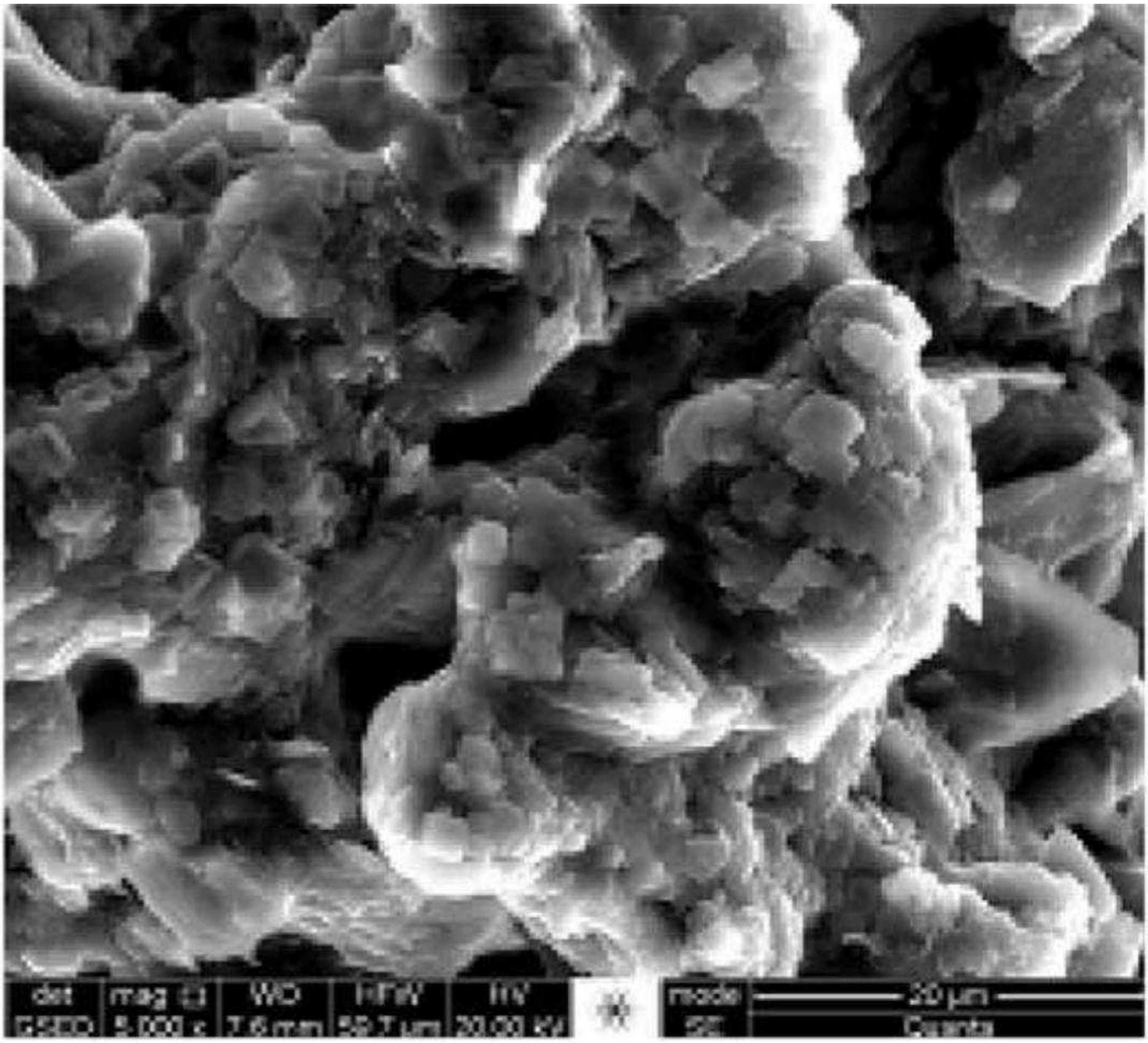

Fig. 2 SEM of artificially structured soils

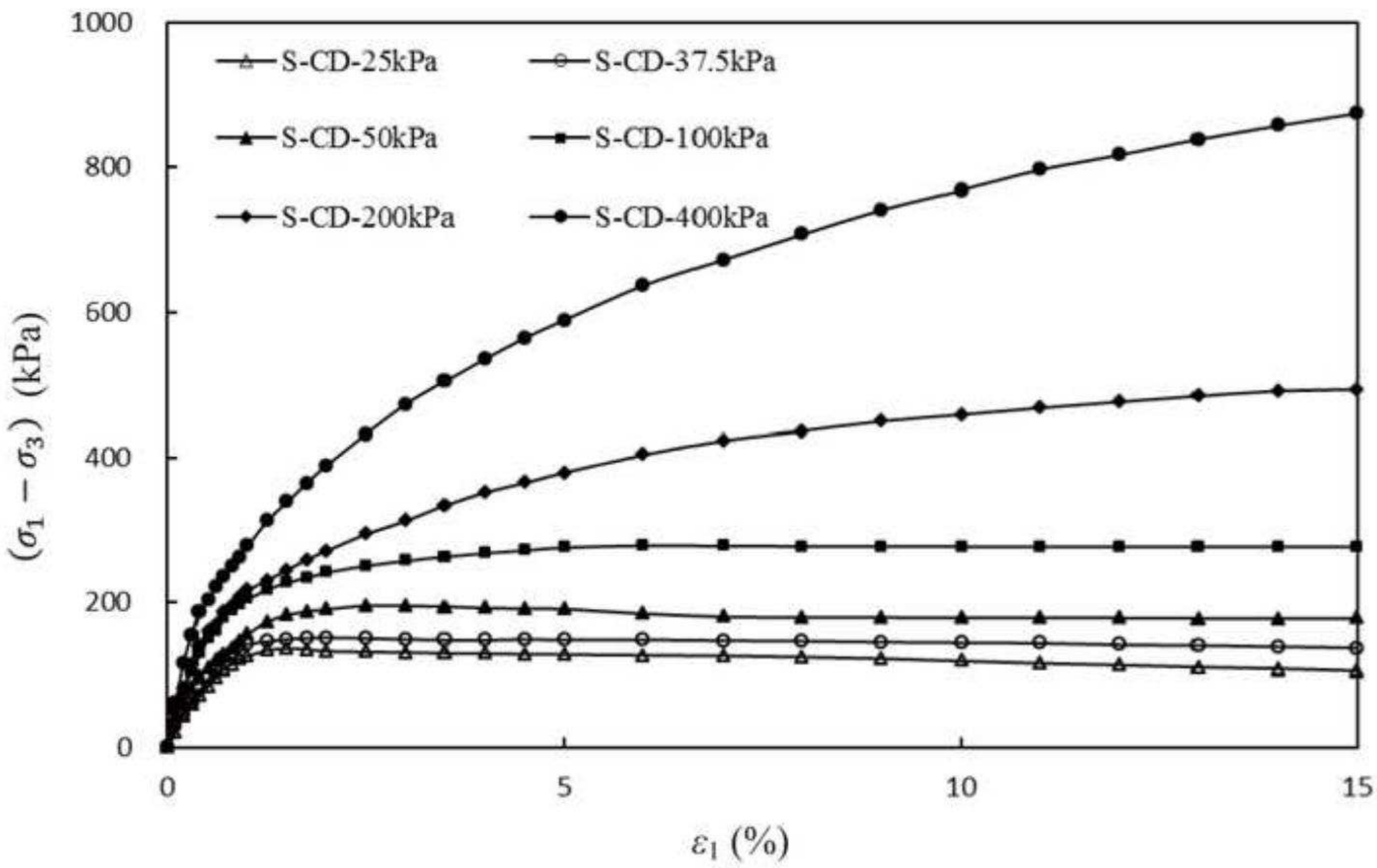

Fig. 3(a) Deviatoric stress - axial strain curves

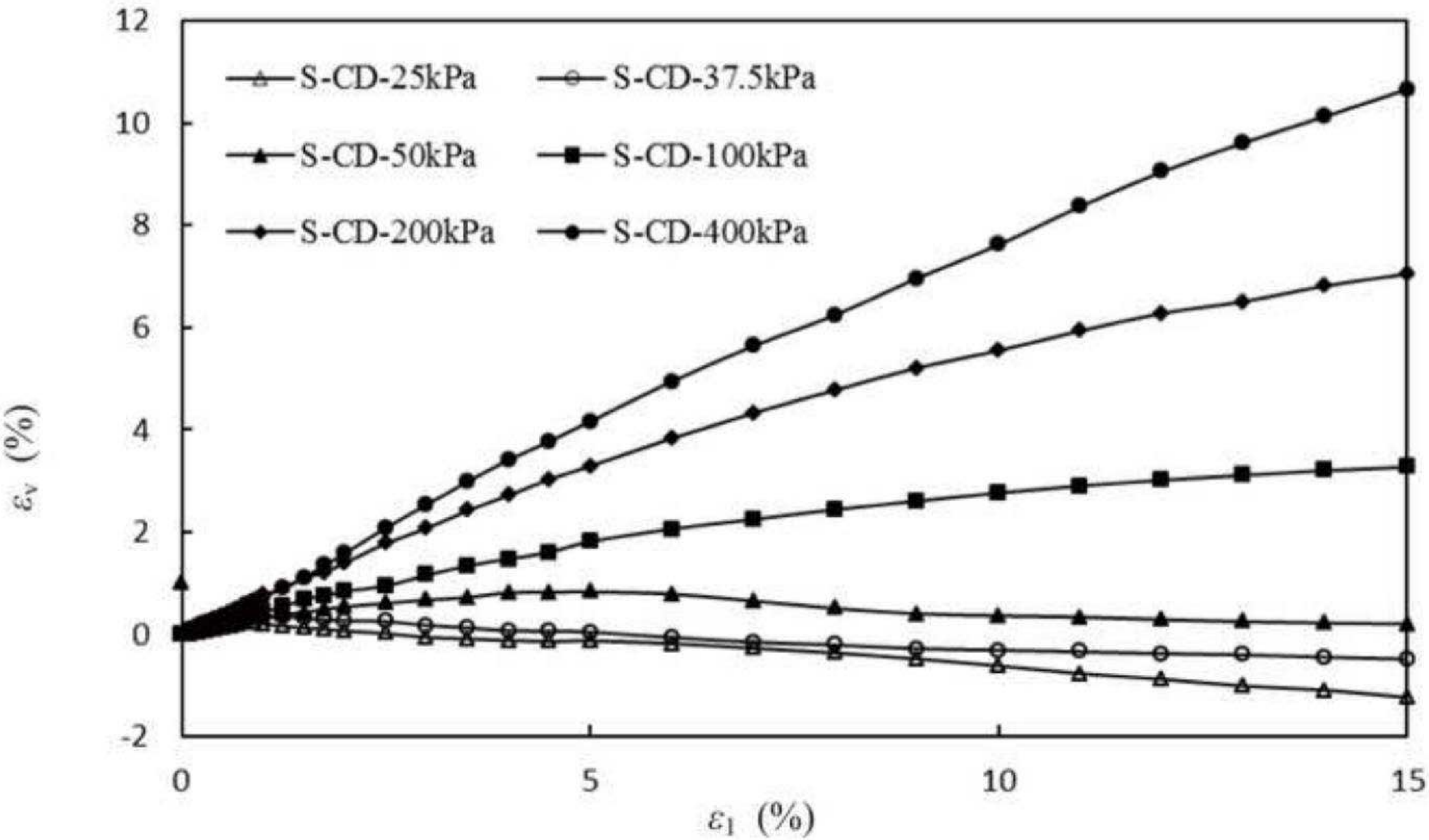

Fig. 3(b) Volumetric strain - axial strain curves

Figure 4

Click here to download Figure FIG.4.TIFF

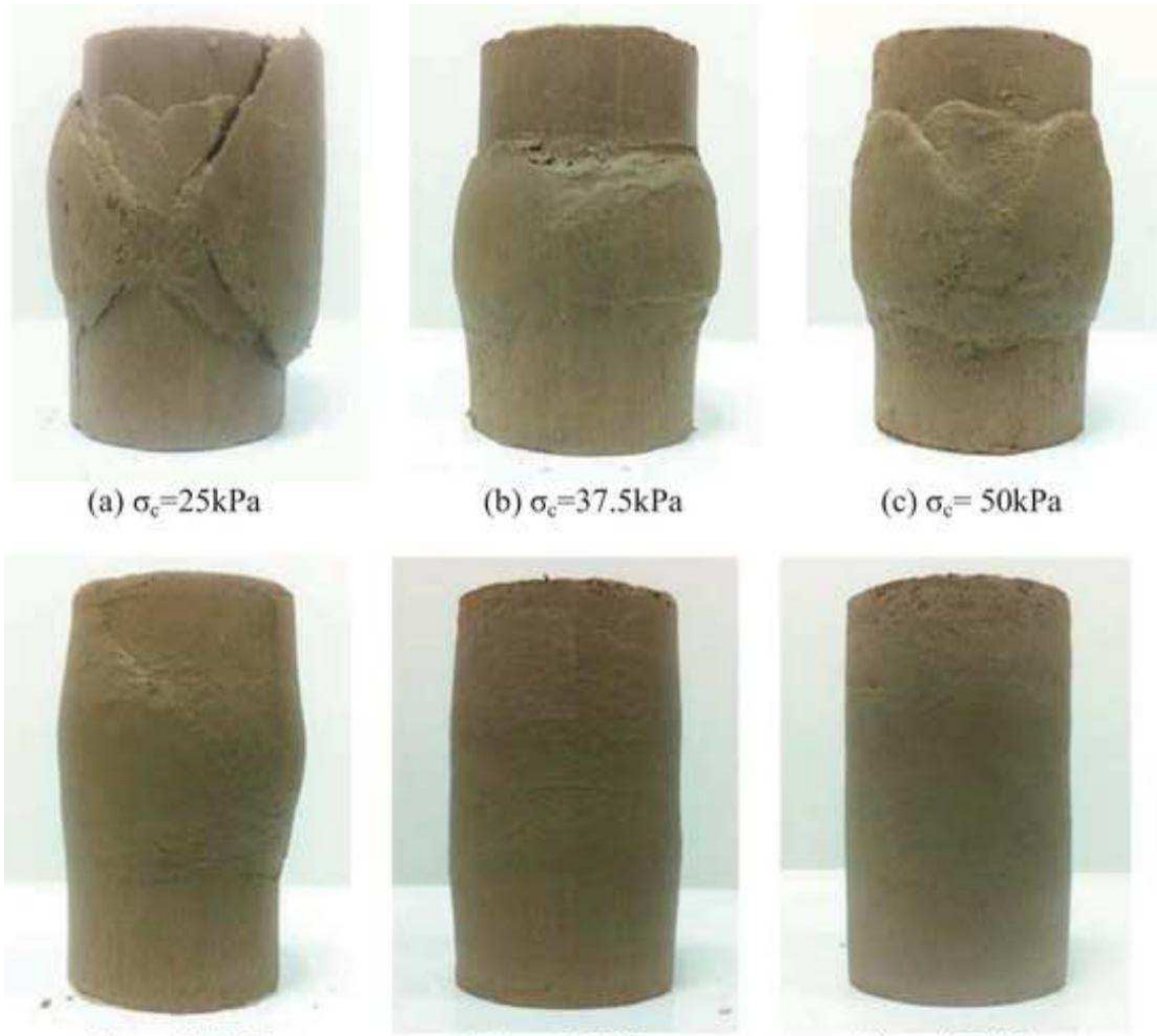

Fig. 4 Failure patterns of structured samples

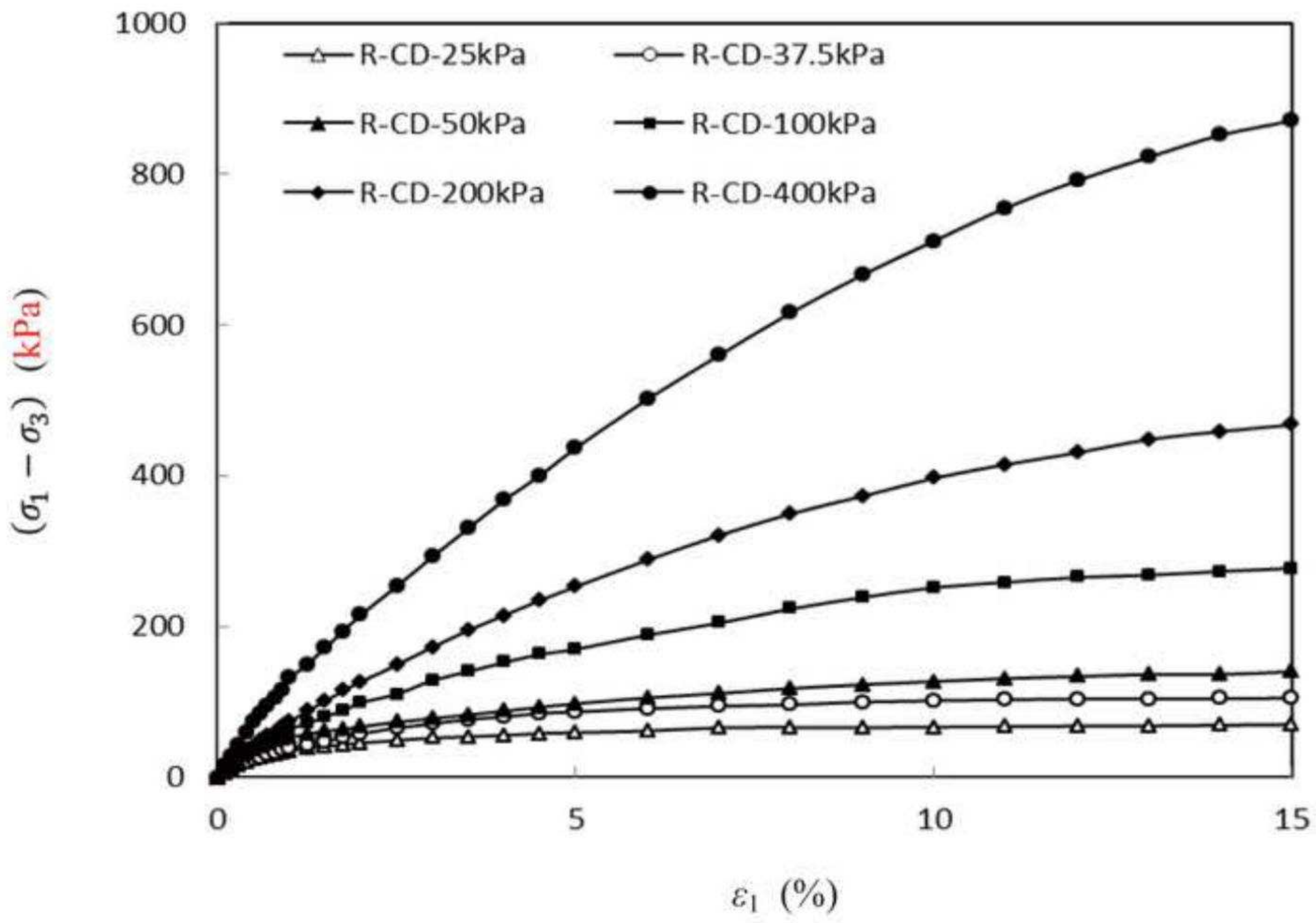

Fig. 5 (a) Deviatoric stress - axial strain curves

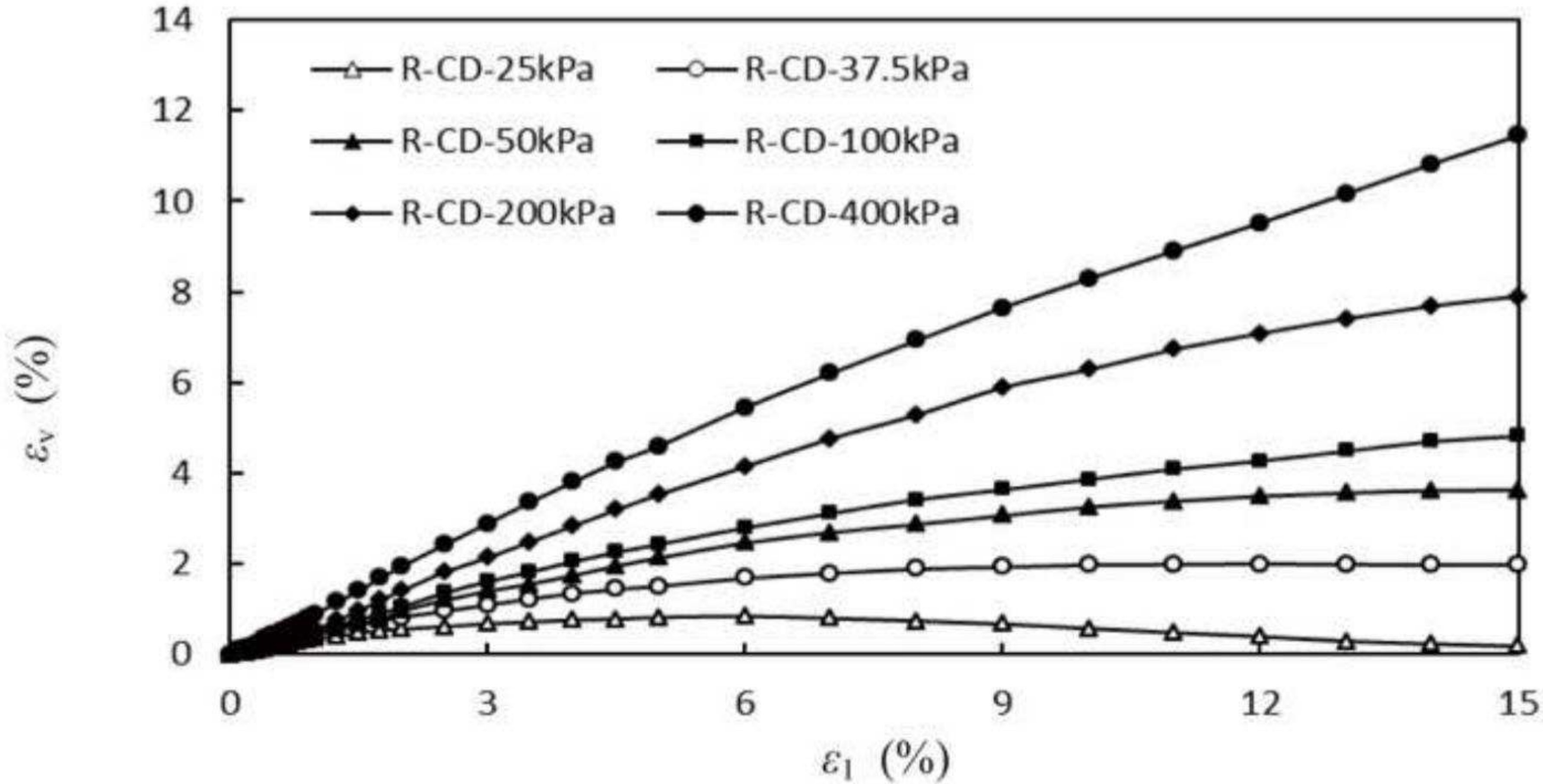

Fig. 5(b) Volumetric strain - axial strain curves

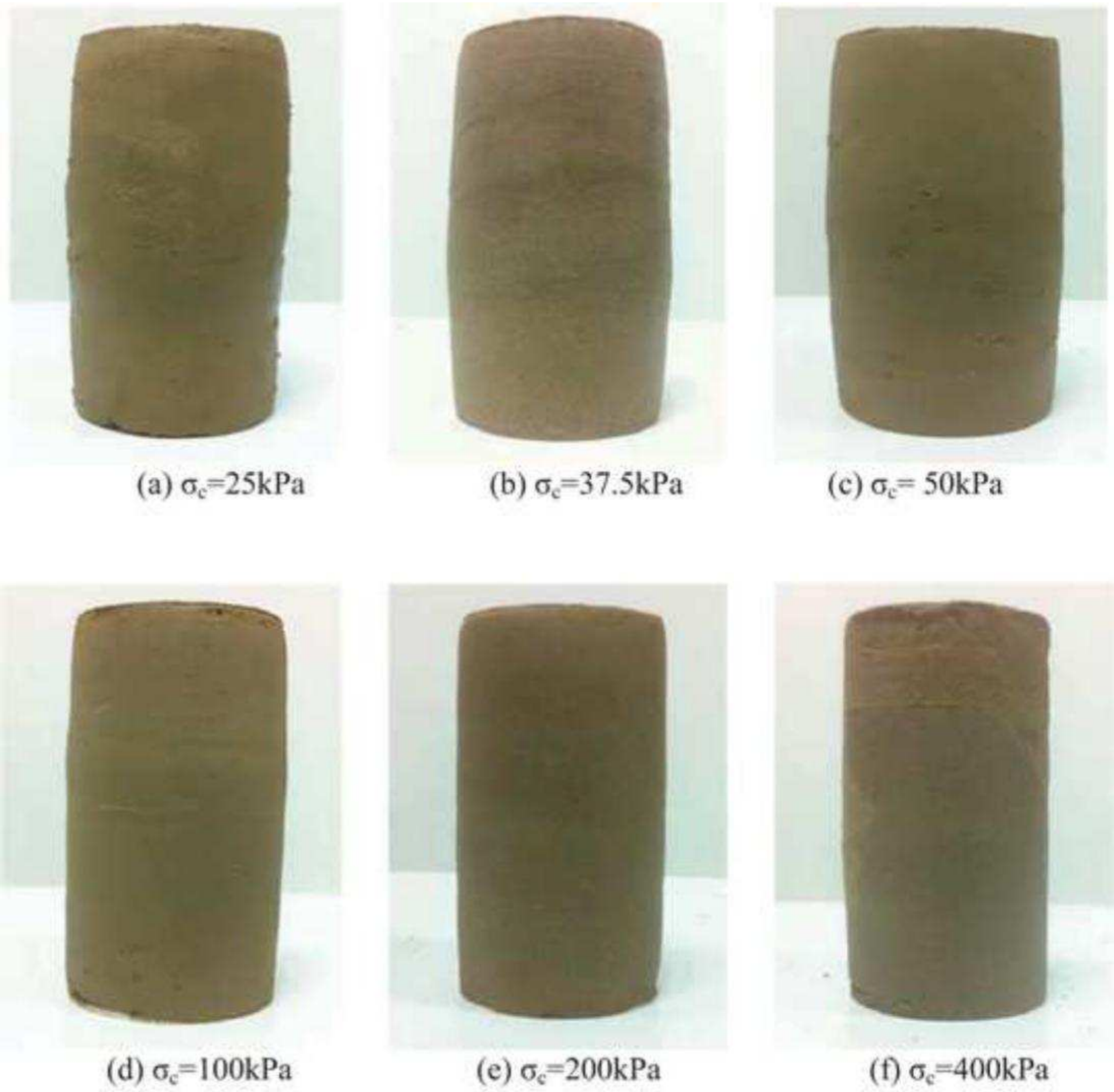

Fig. 6 Failure patterns of remoulded samples

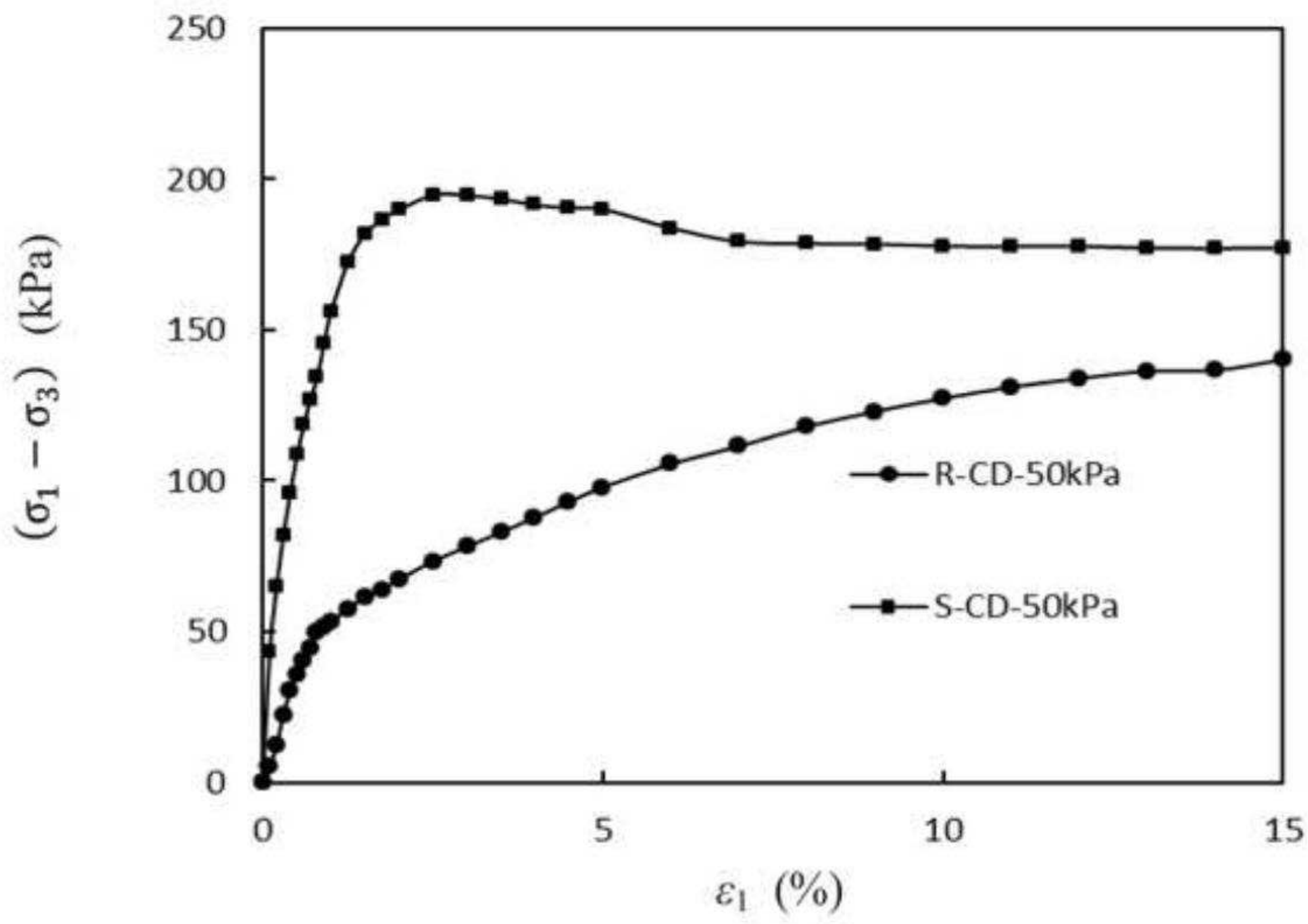

Fig. 7 (a) Deviatoric stress - axial strain curves at 50kPa confining pressure

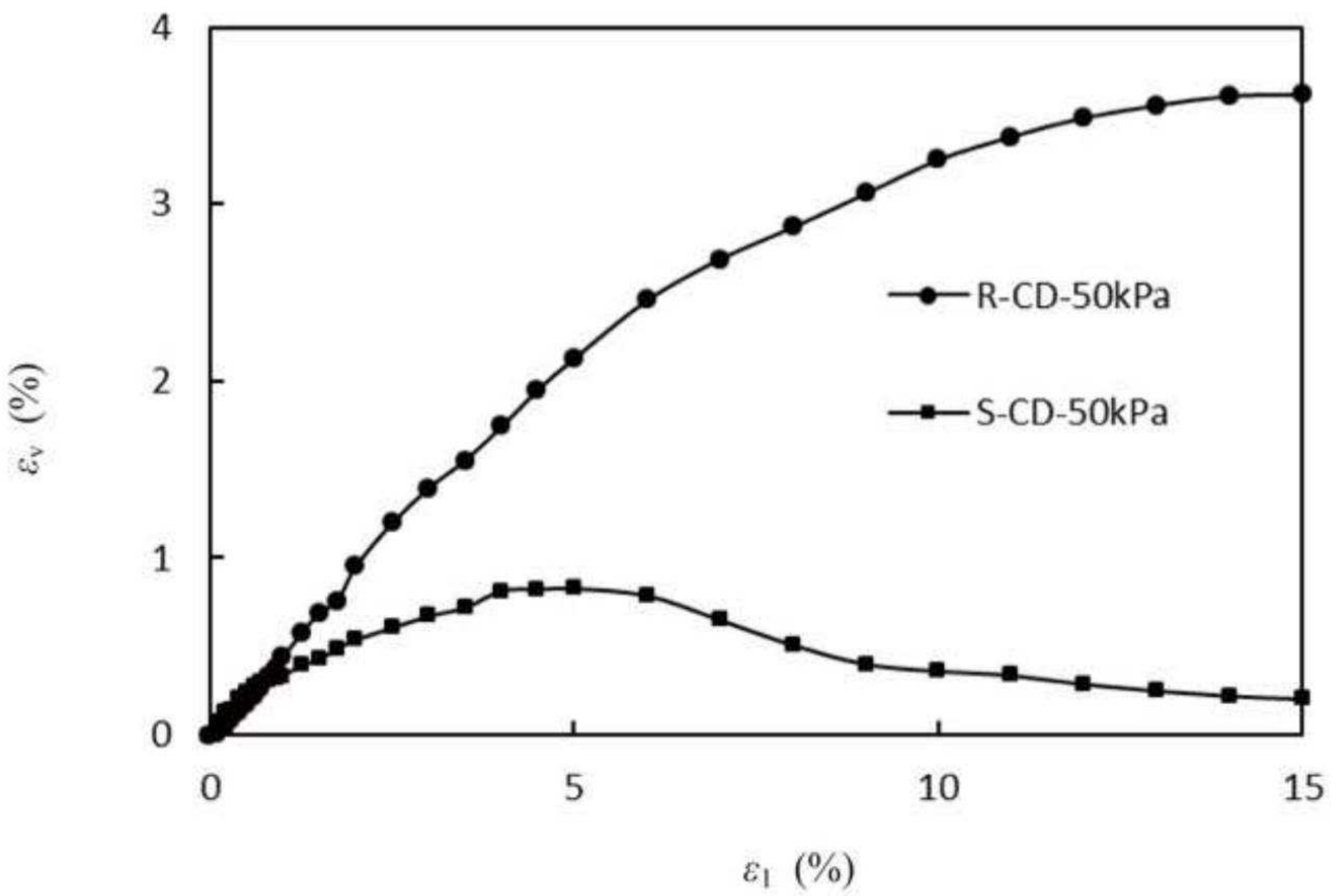

Fig. 7 (b) Volumetric strain - axial strain curves at 50kPa confining pressure

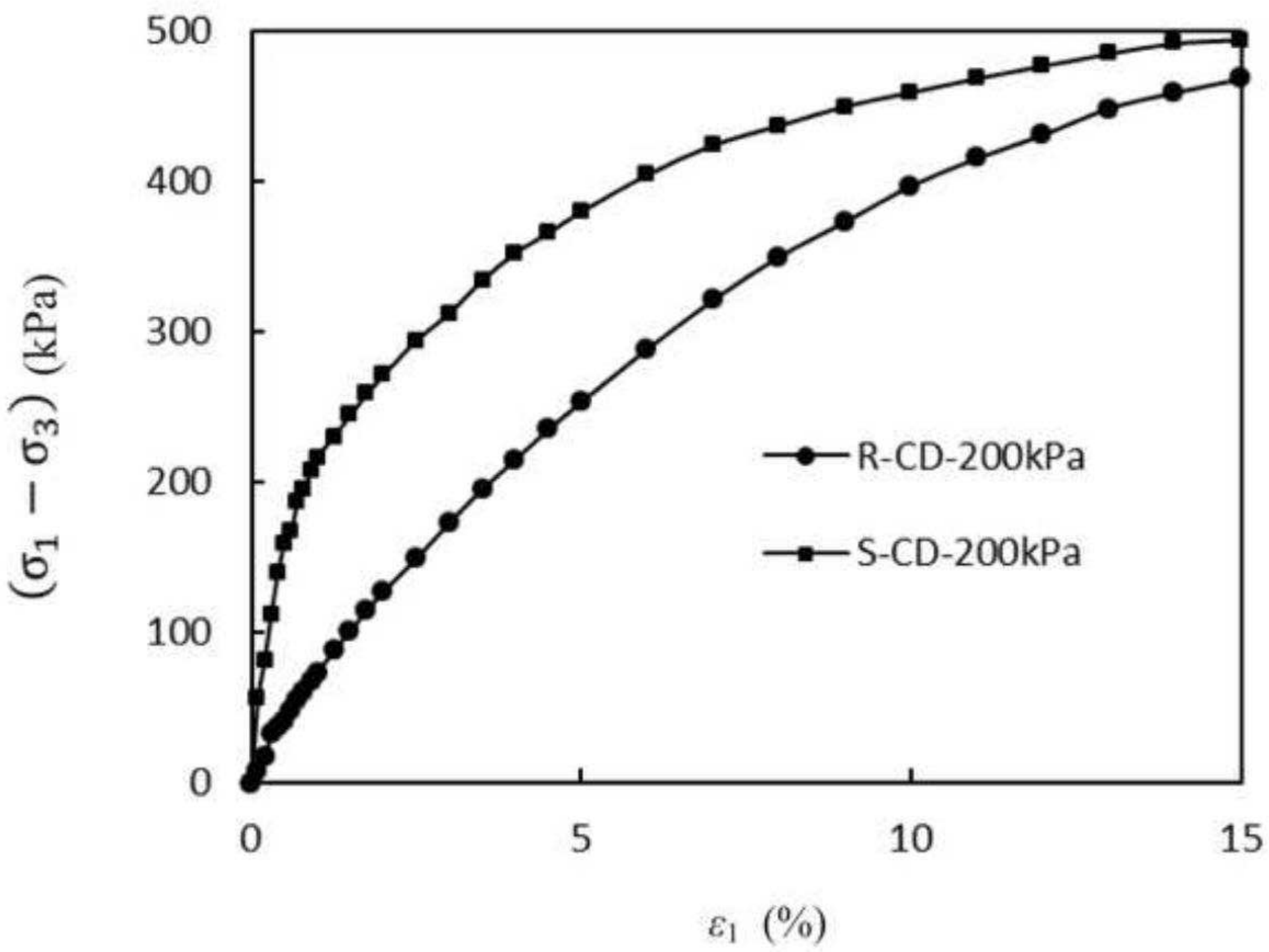

Fig. 8 (a) Deviatoric stress - axial strain curves at 200kPa confining pressure

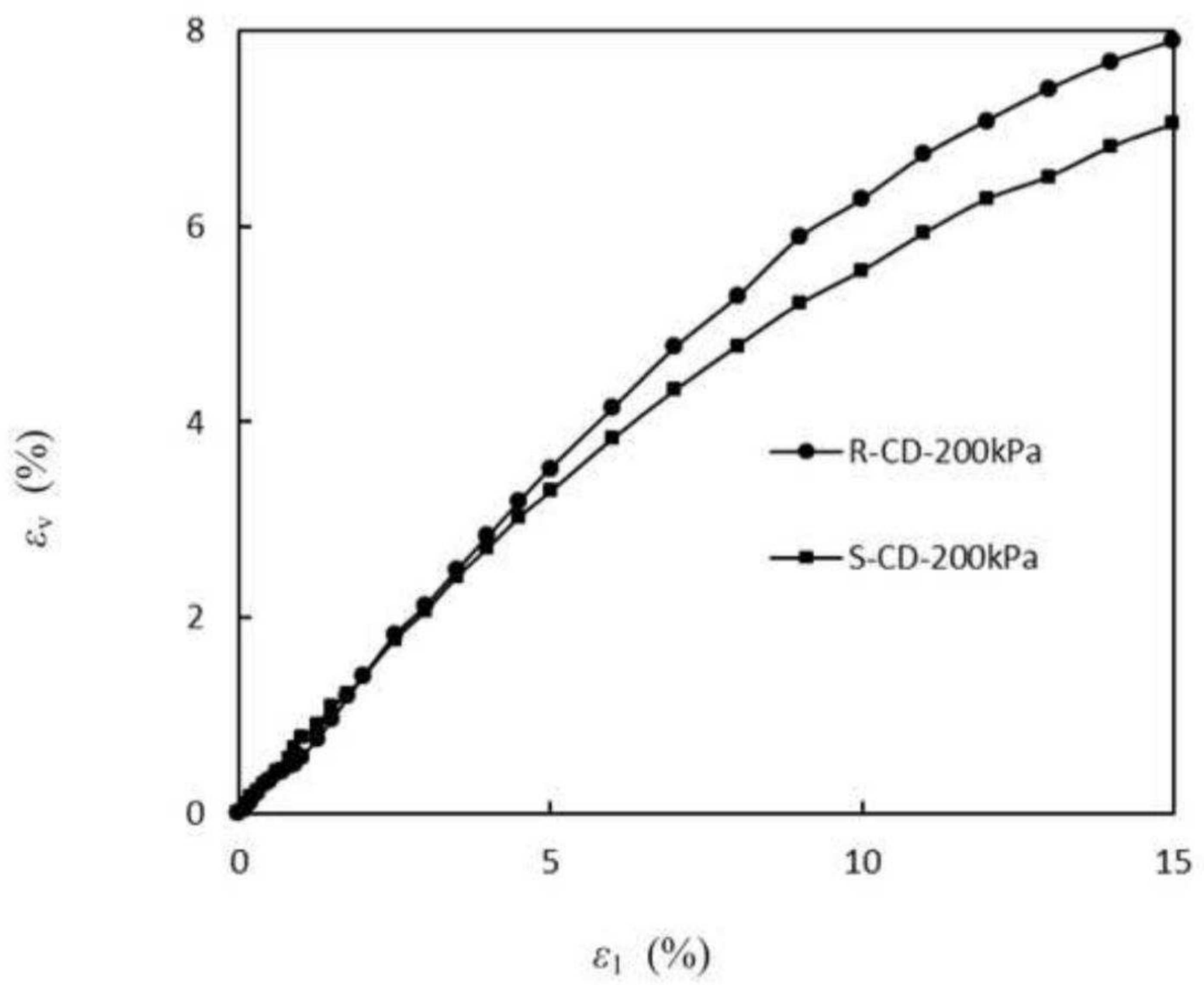

Fig. 8 (b) Volumetric strain - axial strain curves at 200kPa confining pressure

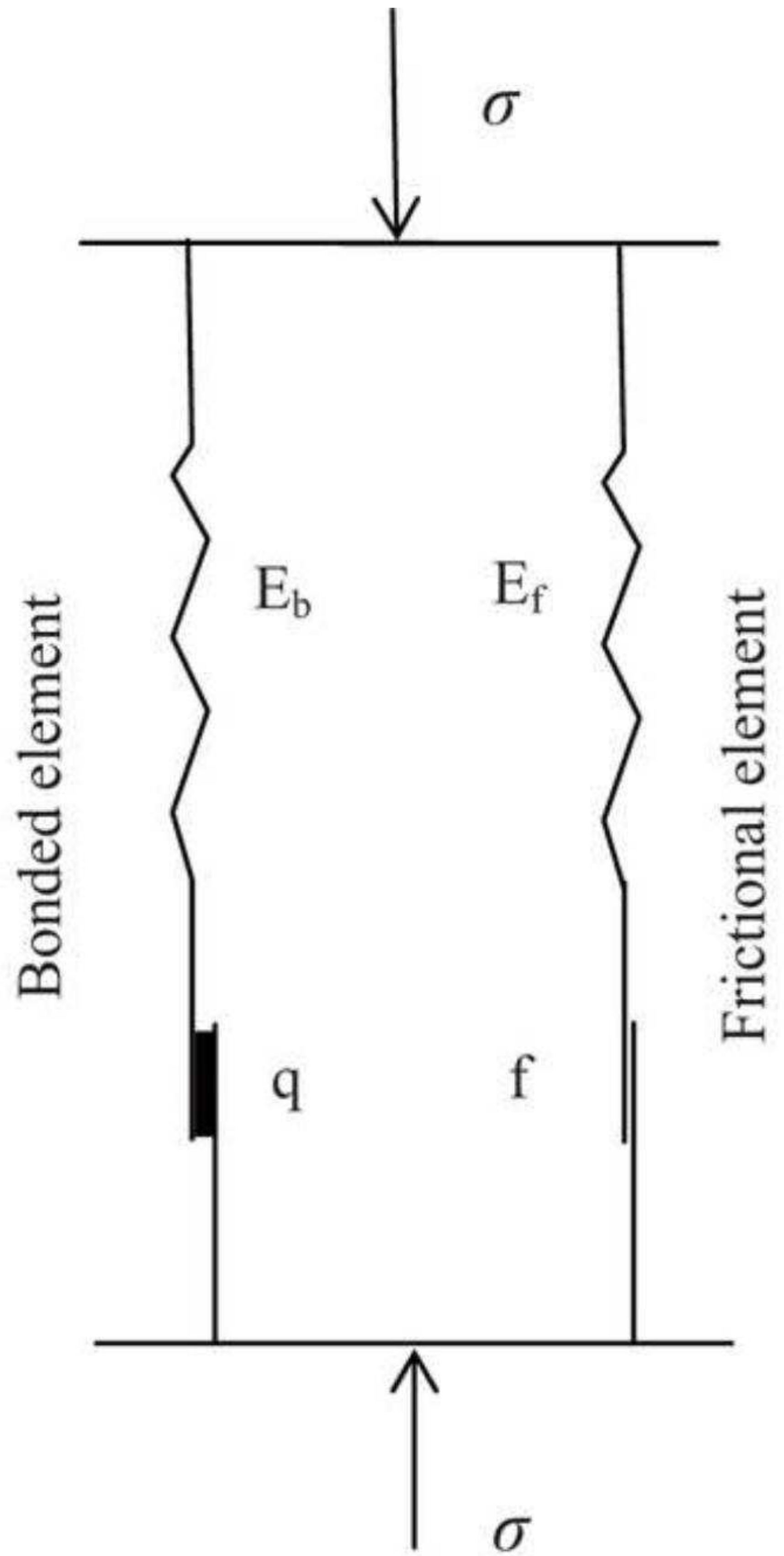

Fig. 9 Sketch of Binary-Medium Material

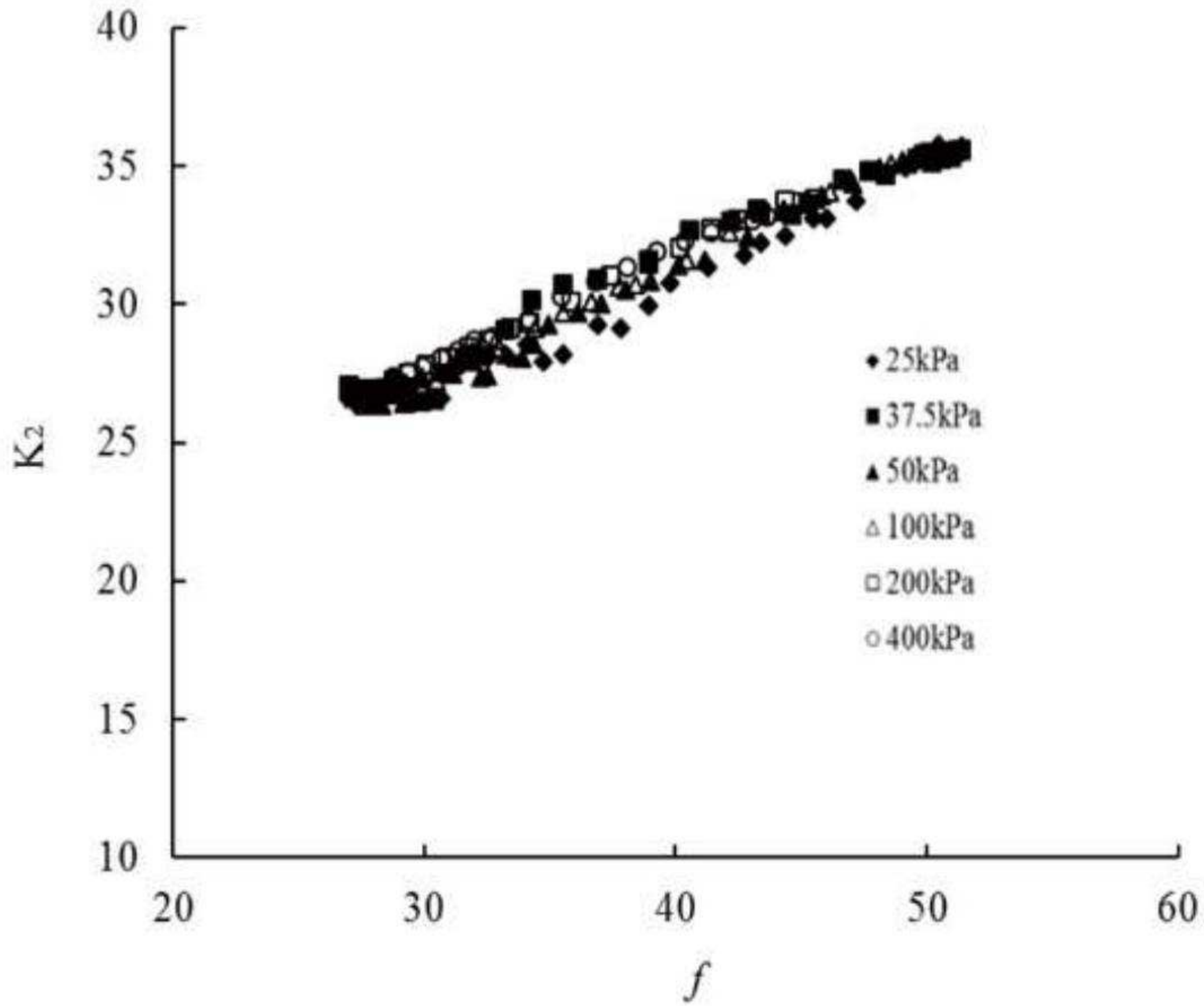

Fig. 10 The relationship curve of $K_2 \sim f$

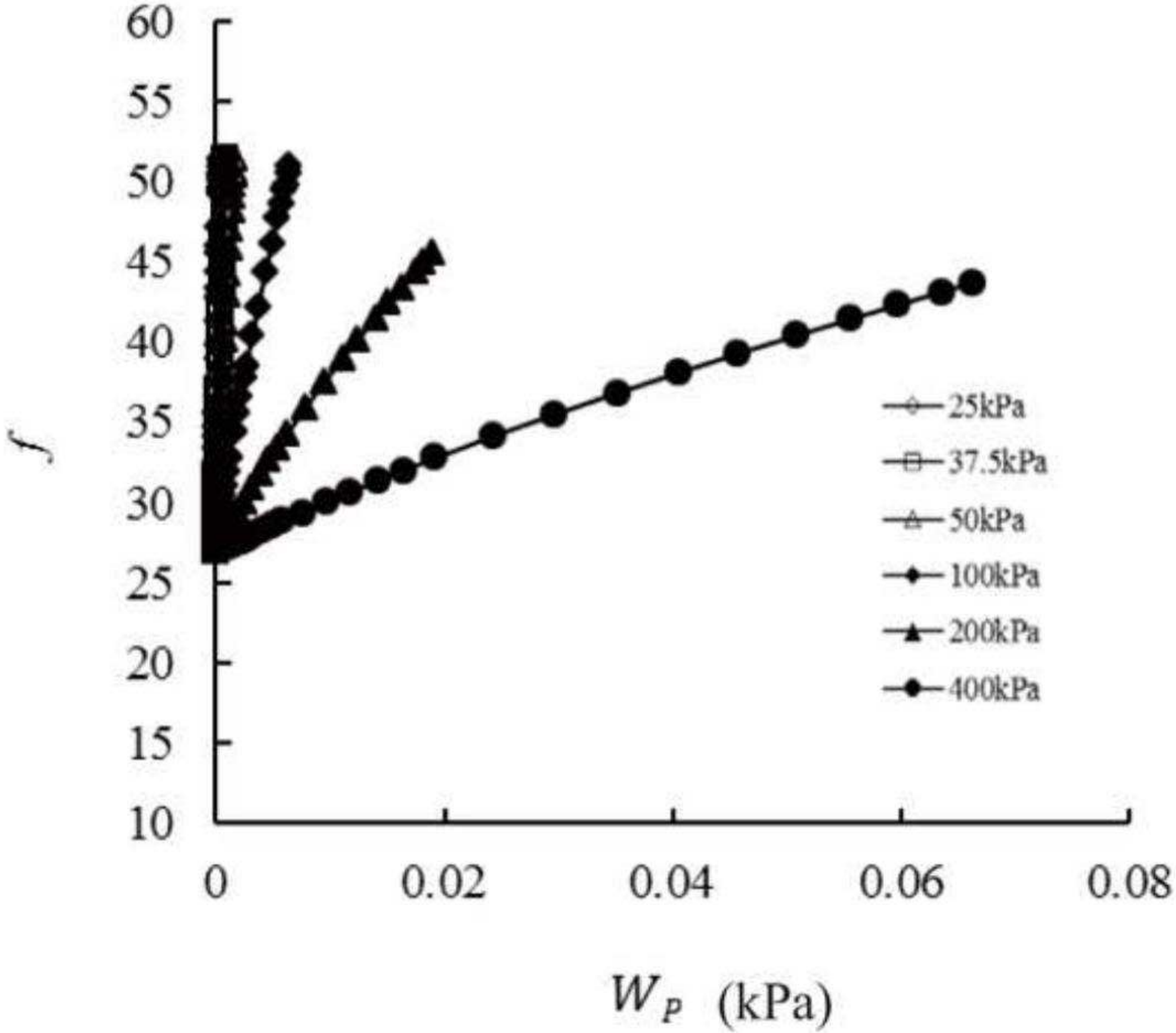

Fig. 11 The relationship curve of $f \sim W_P$

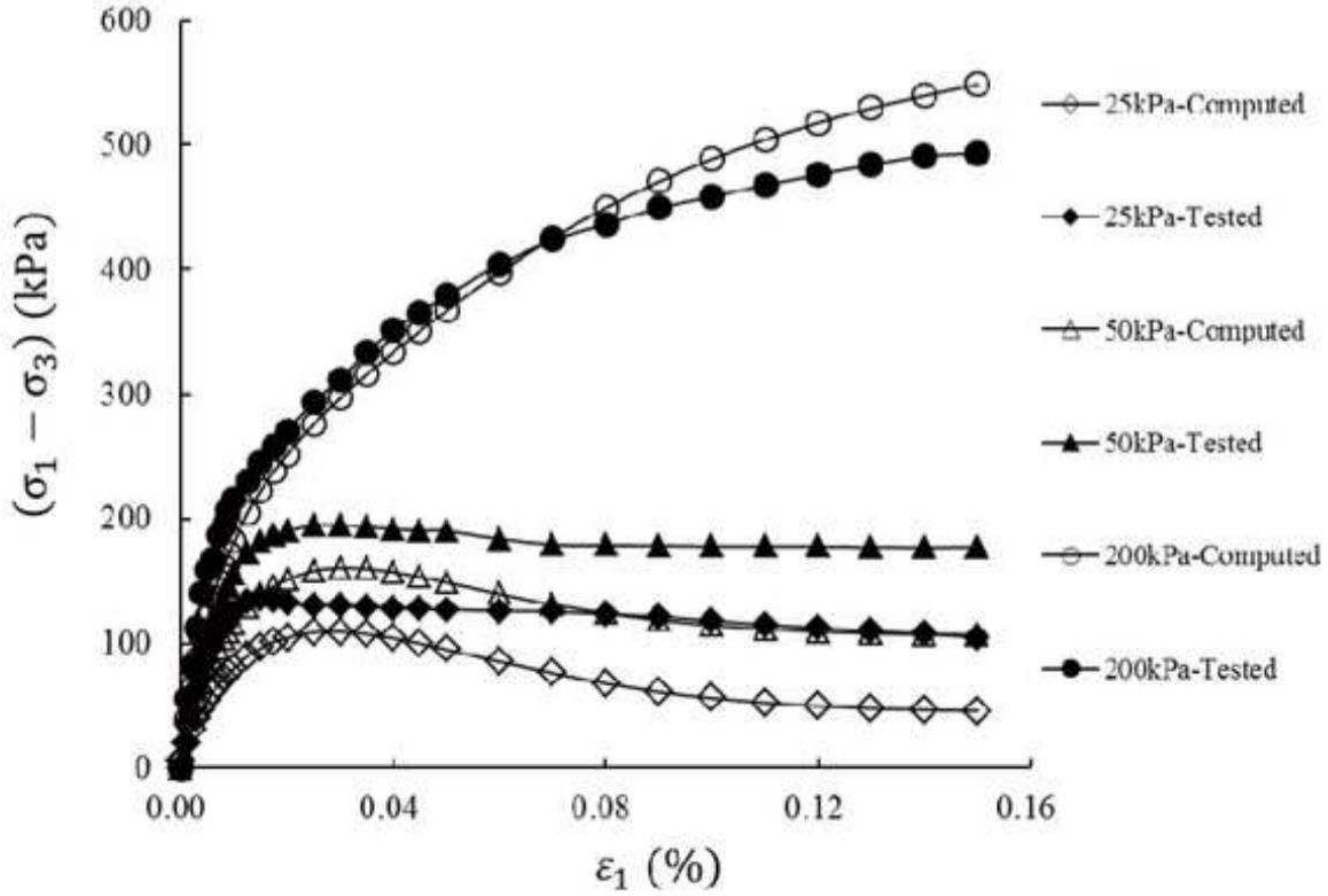

Fig. 12 (a) Curves of deviatoric stress and axial strain tested and computed of structured soils at confining pressures of 25, 50 and 200 kPa

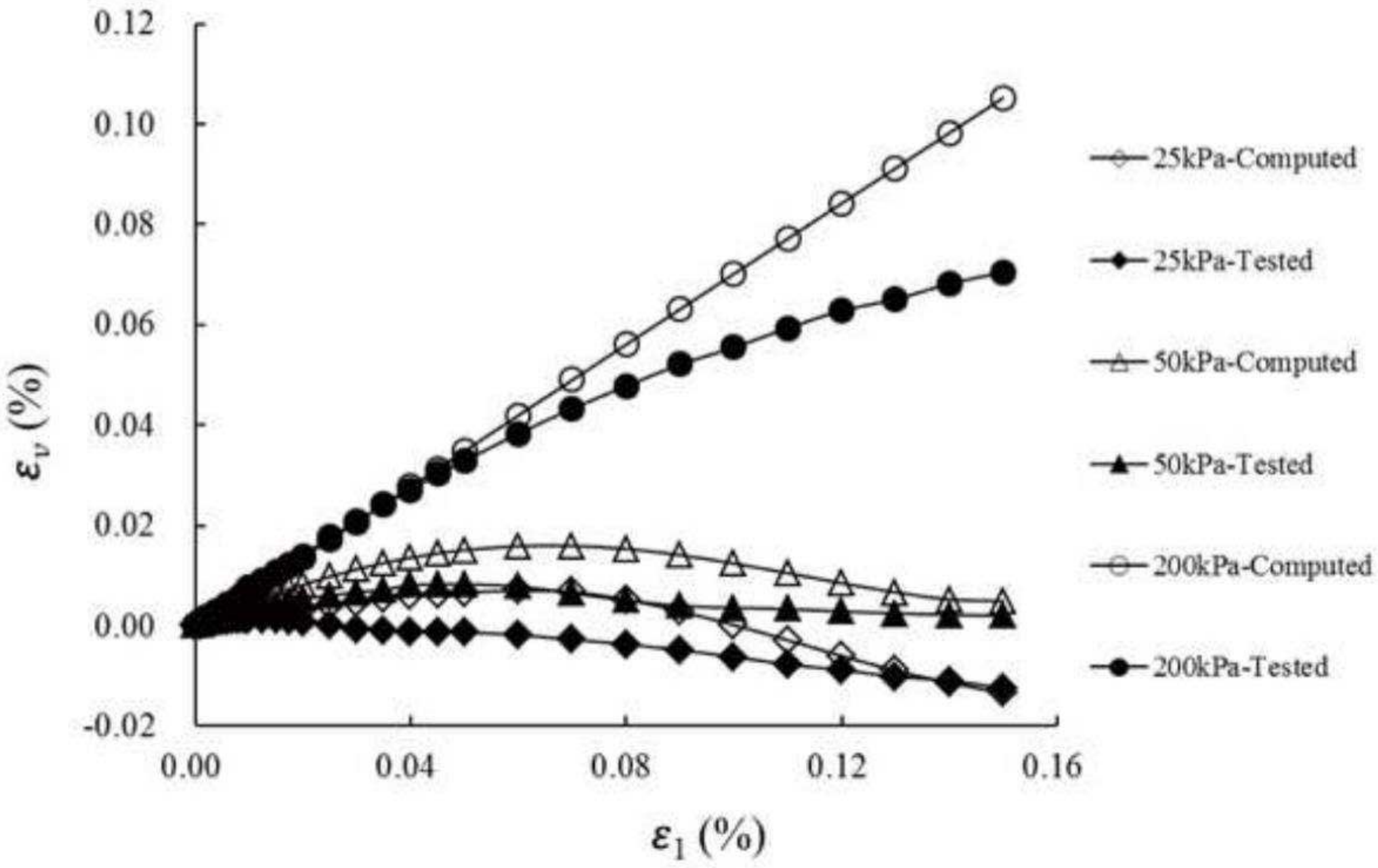

Fig. 12 (b) Curves of volumetric strain and axial strain tested and computed of structured soils at confining pressures of 25, 50 and 200 kPa

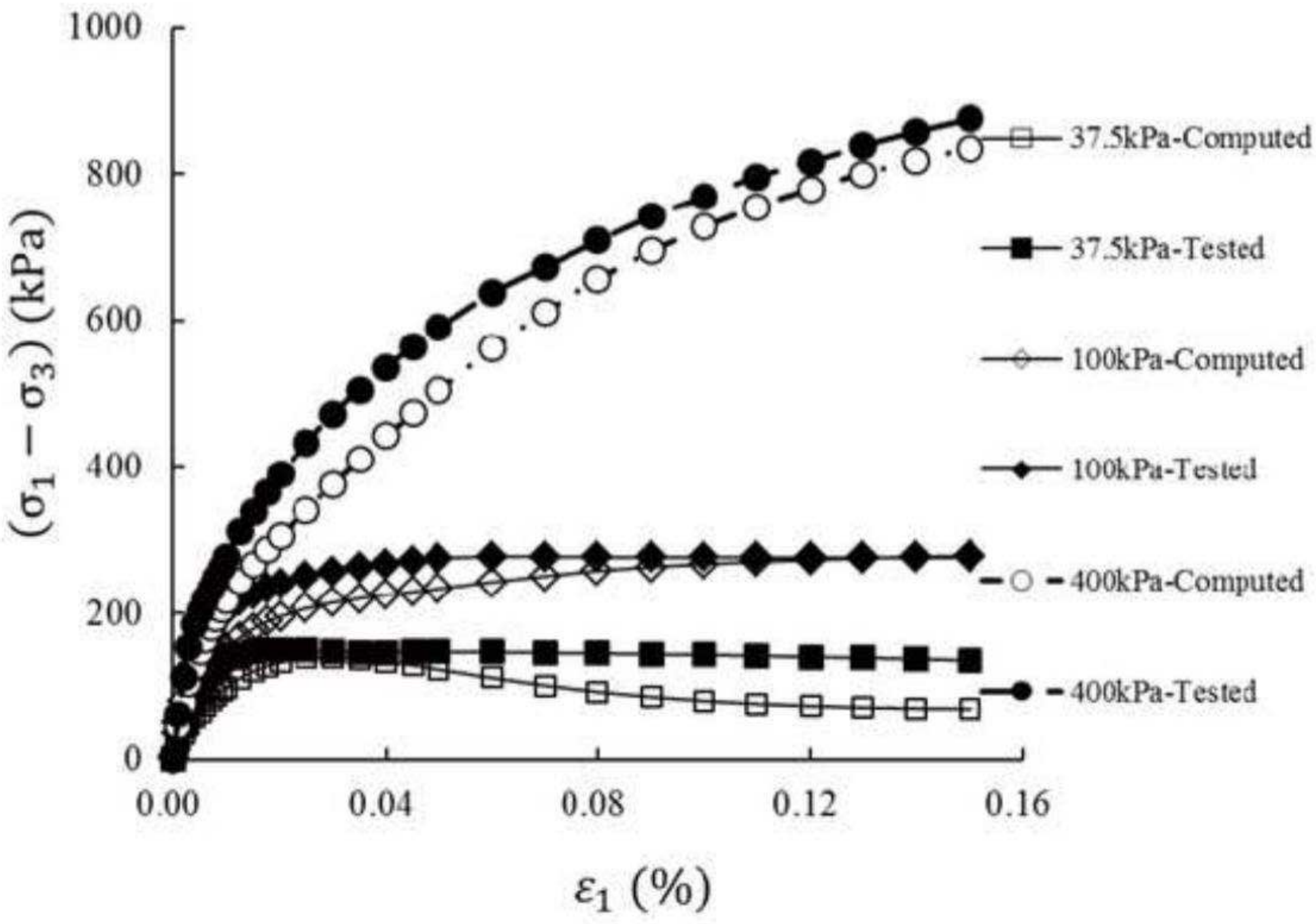

Fig. 13 (a) Curves of deviatoric stress and axial strain tested and computed of structured soils at confining pressures of 37.5, 100 and 400 kPa

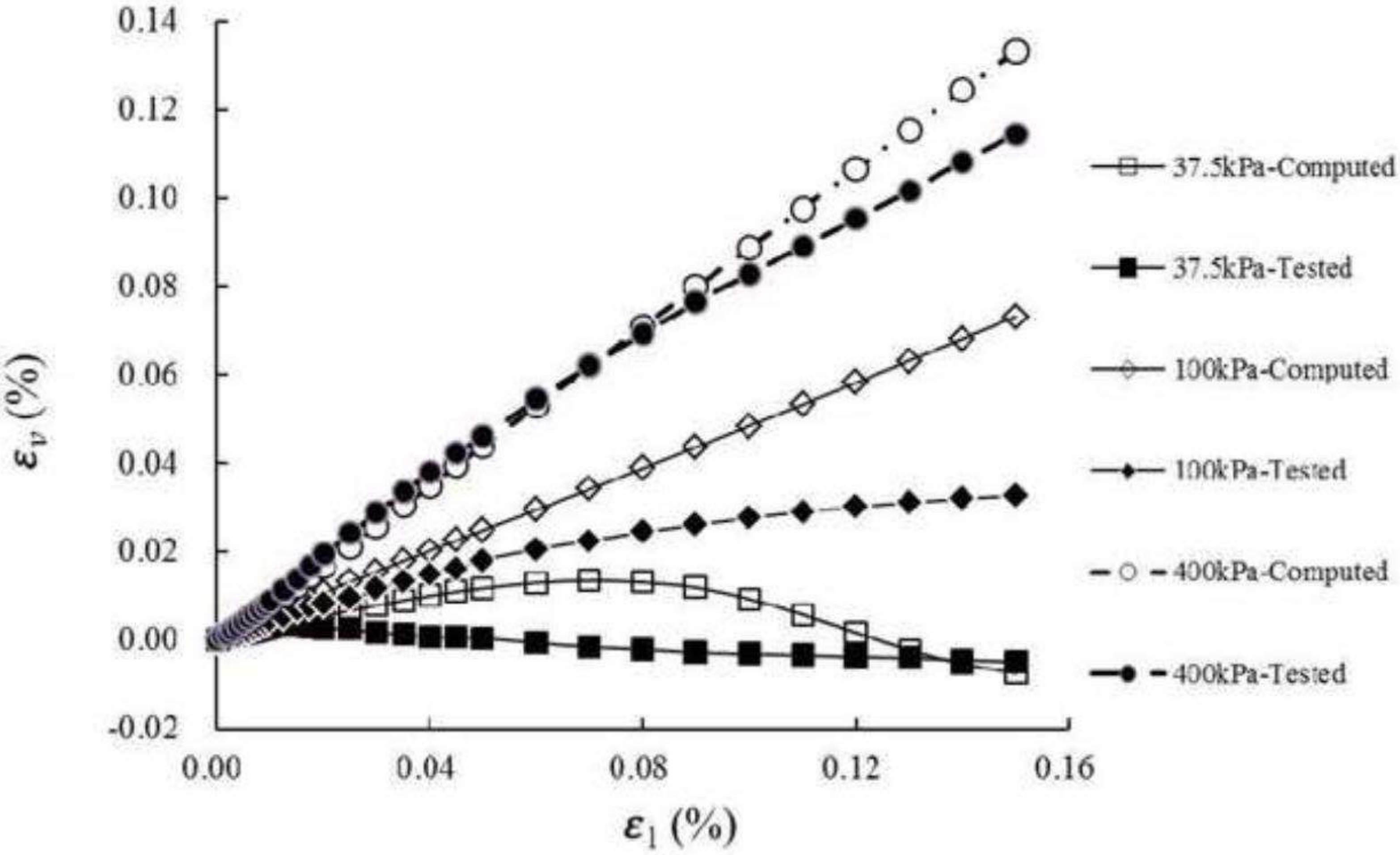

Fig. 13 (b) Curves of volumetric strain and axial strain tested and computed of structured soils at confining pressures of 37.5, 100 and 400 kPa